

QUANTIFICATION OF 3D NETWORK GEOMETRY IN COLLAGEN HYDROGELS



22/06/2016

AUTHOR: ALEJANDRO VIDAL GARCÍA-ARIAS

TUTOR: ARRATE MUÑOZ BARRUTIA

EXTERNAL TUTOR: JAVIER LANILLOS MANCHÓN

ACKNOWLEDGEMENTS

I would like to thank all the people that have collaborated to the project by giving support, help and advice.

Specially, I would like to appreciate to Javier Lanillos for his continuous support and counsel throughout this project, and Arrate Muñoz-Barrutia for her guidance and constructive reviews for the project development. Both contributions have been critical for my personal and professional growth.

ABSTRACT

Cancer is one of the principal causes of death in the world. Despite of the fact that there are ways of fighting the disease, full understanding about cancer cells behaviour is still distant. Extracellular matrix (ECM) is the three-dimensional environment where cells live, and its arrangement is known to modulate cell fate. Study of how ECM-cancer cell interactions affect tumour progression is key for developing more effective drugs to heal cancer. As collagen is the most abundant ECM component, collagen hydrogels can be used as ECM models for research. This bachelor thesis is focused on proposing a processing pipeline for the extraction and characterization of fibre network from collagen hydrogel's reflection microscopy images. This pipeline is composed by an image binarization procedure and a fibre network extraction algorithm from which the network parameters (i.e., fibre length, fibre persistence length, and crosslink density) are computed. The whole pipeline was tested in order to ensure its consistency, and eventually used for the characterization of real collagen hydrogel reflection microscopy images at different gel concentrations introduced in two types of in vitro platforms, culture wells and microfluidic devices. The study showed that fibre length and persistence length are similar for the different concentrations, while the network pore size decreases as the collagen concentration of the hydrogel increases. The future final step of the project would be to introduce cancer cells along with collagen hydrogels in the two platforms, and observe how collagen (ECM) disposition and characteristics direct cancer cell behaviour.

INDEX

ACKNOWLEDGEMENTS	3
ABSTRACT	5
INDEX	8
FIGURES INDEX	10
TABLES INDEX	12
1.BACKGROUND	13
1.1 MOTIVATION	13
1.2 BIOLOGICAL CONTEXT	14
1.2.1. EXTRACELLULAR MATRIX	14
1.2.2. ROLE OF ECM IN CANCER DEVELOPMENT	16
1.3 PROJECT BACKGROUND	18
1.4 OBJECTIVES	19
1.5 STATE OF THE ART	20
2.INTRODUCTION	21
2.1 COLLAGEN HYDROGELS	21
2.2 MICROFLUIDIC DEVICES	23
2.3 REFLECTION AND CONFOCAL MICROSCOPY	23
2.3.1 REFLECTION MICROSCOPY	23
2.3.2 CONFOCAL MICROSCOPY	24
3. MATERIALS AND METHODS	27
3.1 COLLAGEN NETWORK'S PARAMETERS OF INTEREST	27
3.2 ARTIFICIAL IMAGES	28
3.3 PREVIOUS LITERATURE IMAGES	30
3.4 OWN REAL IMAGES	31
3.4.1 COLLAGEN HYDROGELS PREPARATION	32
3.4.1.1 FLUORESCENT COLLAGEN HYDROGELS	33
3.4.2 WELLS AND MICROFLUIDIC DEVICES	33
3.4.3. MICROSCOPY IMAGE ACQUISITION	36
3.5 IMAGE PROCESSING PIPELINE	38
3.5.1 STEERABLE FILTERING	38
3.5.2 IMAGE THRESHOLDING	40

3.6 QUANTIFICATION OF 3D NETWORK GEOMETRY.....	41
3.6.1 DISTANCE FUNCTION	42
3.6.2 NUCLEATION POINTS FINDING	42
3.6.3 FIBER EXTENSION.....	42
3.6.4 FIBERS POSTPROCESSING	43
3.6.5 FIBER PARAMETERS COMPUTATION.....	44
3.5.6 BEAM NETWORK FORMATION	44
3.6.7 PORE SIZE COMPUTATION.....	44
4. RESULTS.....	47
4.1 FIRE PIPELINE EVALUATION.....	47
4.2 FIRE INTERNAL VARIABILITY	56
4.3 PRE-PROCESSING FILTER TESTING.....	57
4.4 PIPELINE TESTING	60
4.5 REAL IMAGES ANALYSIS	64
5. CONCLUSIONS.....	70
6. FUTURE WORK.....	71
7. SOCIOECONOMIC IMPACT	72
8. BUDGET	73
9. ANNEX I (INPUT FIRE PARAMETERS)	74
10. BIBLIOGRAPHY	75

FIGURES INDEX

Figure 1: Extracellular matrix components' connection with cell membrane [6].	15
Figure 2 : Schematic representation of the basic mechanism of a metastasis process [8].	17
Figure 3: a) Collagen synthetization process [13]. b) Collagen structural arrangement [14].	21
Figure 4: Reflection microscopy set up [17].	24
Figure 5: a) Reflection microscopy of sample: blurring in the final image. b) Confocal microscopy: pinhole used, selecting information retrieved [19].	25
Figure 6: Confocal microscopy set up with basic components [20].	25
Figure 7: Persistence length basis [2]	27
Figure 8: Step from binary artificial image to Gaussian smoothed artificial image.	30
Figure 9: Image examples for Dataset I, II and III, from left to right.	31
Figure 10 : Wells culture plate used	34
Figure 11: a) Microfluidic device sketch. b) Real microfluidic device [23].	34
Figure 12: Microfluidic devices production in PDMS [23]: a) Photoresist film addition. b) Mask addition c) UV light applied. d) PDMS curing. e) PDMS removal. f) Inlet channels creation.	35
Figure 13: Sample images of collagen hydrogels with a concentration of 1.5 mg/ml polymerized in wells: a) Reflection Microscopy. b) Confocal microscopy	37
Figure 14: Schematic representation of real collagen hydrogels images (stack of 4 images).	38
Figure 15: Examples of steerable filters masks for feature detection: a, b and c masks correspond to Gaussian steerable filters of first order; d and e masks correspond to Gaussian steerable filters of second order [25].	40
Figure 16: Collagen hydrogel image histogram with its Otsu threshold for binarization.	41
Figure 17: Fibre extension procedure (Circled NP valued 4. Circled NP's LMPs valued 2. Circled LMP of NP's LMP valued 3) [2].	43
Figure 18: Covering radius transform spheres in the fluid phase [11]	45
Figure 19: Exponential length distribution for artificial images.	48
Figure 20: Artificial image examples at the four concentrations.	49
Figure 21: Artificial image dilation.	50
Figure 22: FIRE processing output	51
Figure 23: CDF distribution difference for fibre length and fibre persistence length between the original artificial image, and the results after FIRE processing: a) CDF difference in fibre length for density 1 mg/ml. b) CDF difference in fibre persistence length for density 1 mg/ml.	52
Figure 24 : CDF distribution difference for fibre length and fibre persistence length between the original artificial image, and the results after FIRE processing: a) CDF difference in fibre length for density 1.5 mg/ml. b) CDF difference in fibre persistence length for density 1.5 mg/ml.	53
Figure 25: CDF distribution difference for fibre length and fibre persistence length between the original artificial image, and the results after FIRE processing: a) CDF difference in fibre length for density 2 mg/ml. b) CDF difference in fibre persistence length for density 2 mg/ml.	54
Figure 26 : CDF distribution difference for fibre length and fibre persistence length between the original artificial image, and the results after FIRE processing: a) CDF difference in fibre length for density 2.5 mg/ml. b) CDF difference in fibre persistence length for density 2.5 mg/ml.	55

Figure 27: a) Real image. b) Gaussian filtered image. c) Otsu binarization of Gaussian filtered image. d) Median filtered image. e) Otsu binarization of Median filtered image. f) Steerable filtered image. g) Otsu binarization of steerable filtered image.....	59
Figure 28: Maximum CDF difference between the three datasets for fibre length. Original results (a) and reproduced results (b).....	62
Figure 29: Maximum CDF difference between the three datasets for fibre persistence length. Original results (a) and reproduced results (b).	63
Figure 30 : Example of confocal fluorescence microscopy for collagen hydrogels.	64
Figure 31: Examples of confocal reflection microscopy images for collagen hydrogels.	65
Figure 32 : Fibre extraction by FIRE [3].	66
Figure 33 : Mean fibre length distribution vs concentration.	67
Figure 34 : Mean fibre persistence length distribution vs concentration.	67
Figure 35: Mean pore size distribution vs concentration.	68
Figure 36: Crosslink density distribution vs concentration.....	68

TABLES INDEX

Table 1: For each collagen type, the tissues in which they are present and the cells of origin are listed [4].....	22
Table 2: Volume of reagents needed for preparing each concentration, starting from a 3.43 mg/ml collagen I rat tail stock at pH=2.	33
Table 3: Real images acquisition parameters	37
Table 4: Pore size difference between the original artificial images and the FIRE extracted networks.....	56
Table 5: Maximum difference in parameters computation for similar implementations.....	57
Table 6: Mean fibre length for the three image datasets.....	60
Table 7: Median persistence length for the three datasets.	60
Table 8: Pore size mean for the three datasets.	61
Table 9 : Bachelor thesis budget.....	73

1.BACKGROUND

In this chapter, an introduction to the project object of this bachelor thesis is given. It will consist of: The motivation that originates the project; the biological context that surrounds all the work performed; a description of all the project background; the main objectives to be achieved during this bachelor thesis; and finally, a brief summary of the state of the art regarding this research work.

1.1 MOTIVATION

Cancer is one of the most widespread diseases nowadays, being the main cause of natural death along with cardiovascular diseases in the first world countries according to the World Health Organization [1].

Despite of the fact that there are available several types of treatments in order to fight cancer, there is a real need for the development of more effective drugs to kill cancer cells. The principal drawback of the current treatments is the lack of specificity to attack just cancer cells, which leads to strong side-effects in patients. Hence, the main aim of the pharmacological industry is to create new specific drugs that attack certain features of cancer tumours. In that sense, understanding the complexity of the behaviour and physiology differences among normal cells and cancer cells is a key issue.

One of the main features that affect the fate of each cell is the interaction established between the membrane receptor proteins of the cell and the extracellular matrix components. Cells are not isolated entities in the tissues, they require inputs from other cells but at the same time from the extracellular components, proteins and polysaccharides that conform the extracellular mesh, and which are tightly connected with the cell membrane. That unions or separations between the membrane and the extracellular molecules may induce internal signalling pathways in cells that may lead to differential gene expression, affecting hence any function of the cell, from metabolism to proliferation. As in normal cells, arrangement of the extracellular matrix affects the actions of cancer cells, especially in terms of differentiation of cancer stem cells, proliferation and metastasis.

Consequently, it would be very useful for the biomedical field in cancer research, to have a reliable tool that is able to analyse what are the changes in the extracellular matrix arrangement when a cancer cell interacts with it. This line of study has become very popular nowadays and many papers have arisen describing complex algorithms to extract the 3D network geometry of collagen gels from 3D confocal microscopy images of these gels [2][3]. Collagen hydrogels are used as extracellular matrix models because collagen is the most abundant extracellular matrix protein [4] and it is simple to make it polymerize to form of hydrogels; thus, hydrogels can mimic extracellular matrix mechanical properties. The most relevant and complete algorithm

implemented for the purpose mentioned before is **FIRE** (FibeR Extraction algorithm), which was developed by Andrew Stein from the University of Michigan [2].

This software routine is the one used for the study of collagen gel images in this bachelor thesis. **It allows the reconstruction of fibre network geometry from 3D images. In addition, some fibre parameters like fibre length and fibre persistence length can be computed in order to characterize the network.**

1.2 BIOLOGICAL CONTEXT

1.2.1. EXTRACELLULAR MATRIX

Cells are not isolated systems in the body, they need living basis support and also external signalling supply from other cells or tissues. **Extracellular matrix (ECM) is a collection of extracellular molecules secreted by cells that provide structural and biochemical support to the surrounding cells** [5]. The ECM is produced by fibroblast and is composed by a mixture of components secreted by cells, mainly structural proteins and polysaccharides. So, its main function is serving as support for tissues by absorbing mechanical loads. However, at the same time, the high water component of ECM allows the diffusion and transport of substances through it, so ECM is as well the carrier for all the molecules needed for cell activity. At the same time, the components that integrate the ECM can establish connections with the cell membrane components in order to influence cell behaviour. The relation between the cells and the extracellular matrix is reciprocal, cells regenerate ECM components and meanwhile ECM components intervene in cellular fate.

The ECM is composed by two phases:

- **Basement membrane**: A thin layer of tissue that separates the connective tissue from epithelium, mesothelium or endothelium, to which it is associated. Its main function is to attach the connective tissue to the associated tissue, as well as acting as a key factor for angiogenesis and proliferation. The high density of fibres in this layer makes it act also as an immunological barrier.
- **Interstitial matrix**: It has the form of a hydrogel, composed by high water content and structural peptides and polysaccharides. Its main function is to act as a mechanical support for tissues absorbing loads. The main components of this phase are:
 - o **Collagen**: The most abundant and important protein in the ECM. It gives the matrix the stiffness and mechanical strength.
 - o **Elastin**: Protein that provides the tissue with elasticity, indispensable for deformable organs like the skin.

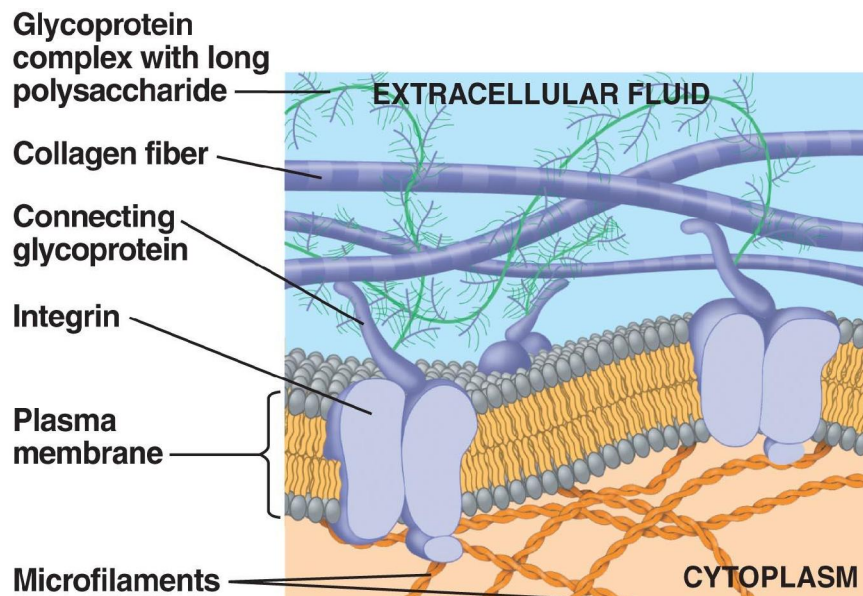


Figure 1: Extracellular matrix components' connection with cell membrane [6].

- o **Fibronectin:** Glycoprotein that binds both, extracellular collagen and integrin, a cell membrane protein.
- o **Laminin:** Forms networks in basal lamina, accounting for tensile strength.
- o **Glycosaminoglycans (GAGs):** Polysaccharides that bind to ECM proteins. Their function is to store molecules, especially water and growth factors. The most notable examples of glycosaminoglycans are heparin sulfate and keratan sulfate.
- o **Hyaluronic acid:** Polysaccharide present in the ECM but not bounded to ECM proteins. Its main function is to give the ECM the ability to allow compression.

This complex composition gives to the ECM the following properties:

- **Mechanical and support properties:** ECM provides a support frame for tissues, allowing them to have some elasticity and tensile strength thanks to elastin and collagen, respectively. At the same time, as mentioned before, hyaluronic acid provides the ECM with the capability of bearing compression. All these mechanical properties are known to affect surrounding cells, regulating cellular behaviour.
- **Effect on surrounding cells' differentiation and gene expression:** Integrins are transmembrane receptors that are the bridges for cell-cell and cell-extracellular matrix (ECM) interactions (see Figure 1). When triggered integrins in turn

trigger chemical pathways to the interior (signal transduction) such as the chemical composition and mechanical status of the ECM, which results in a response (activation of transcription) which affect cell behaviour (i.e., differentiation, migration, metabolism, proliferation). However, cell migration is the most important effect when talking about cancer and tumours spreading in metastasis. That migration is called durotaxis, and it is produced by microkeleton rearrangement. Microkeleton rearrangements occur when specific interactions between ECM anchoring proteins and cell membrane integrins arise, which induces intracellular signalling pathways that lead to cell migration.

1.2.2. ROLE OF ECM IN CANCER DEVELOPMENT

Cancer is a set of hundreds of diseases that are related to an uncontrolled proliferation of cells forming tumours [5]. Cancer is usually produced by accumulation of mutations in cells, because of inheritance, chemical agents or radiation. Nowadays, cancer can be treated by chemotherapy or radiotherapy with a high rate of survival. Nevertheless, these types of treatments are fairly aggressive since they are rather unspecific to the tumours producing terrible side effects in patients. Thus, there is a need to better understand the complex mechanisms that govern cancer cells and their environment in order to be able to design more specific drugs that take advantage of certain cancer cells features.

As explained before, ECM components are key factors in terms of cell regulation. The mechanical behaviour they create in the tissue plus the direct connections with the cell membranes sets up a way of controlling cell behaviour and shape. The main functions that are affected by ECM are: cell migration, cell differentiation, cell metabolism, cell gene expression and cell proliferation.

Focusing in cancer, ECM is an indispensable component in cancer development. ECM forms the stem cell niches of cancer stem cells [7]. Stem cell niches are three-dimensional environments that surround stem cells, and regulate their behaviour in terms of differentiation and proliferation. Abnormal ECM distribution or inability of connection between ECM and stem cells both result on an undesired proliferation of stem cells. This uncontrolled proliferation is based on symmetric divisions (normal mitotic divisions), so no stem cell differentiation occurs. Cancer is the clinical name given for that type of conditions.

ECM affects several tumour parameters:

- **Angiogenesis and lymphangiogenesis:** Tumour cells produce vascular endothelial growth factors (VEGF) and angiogenic ECM fragments to regulate blood vessel's creation. Along with angiogenesis, ECM affect lymphangiogenesis, however, the exact mechanisms are not completely

discovered. Both angiogenesis and lymphangiogenesis are important for tumour proliferation and expansion, as they allow tumours to receive more blood inputs and perform cell infiltration in blood for metastasis.

- **Inflammation:** ECM components in cancer stem cell niches act as chemoattractant for immune system cells and they help immune cells for extravasation in tumour tissue. ECM cells activate macrophages in tumour, that are transformed in tumour associated macrophages promoting tumour proliferation.
- **Progression:** Keeping normal extracellular matrix dynamics is key for maintaining healthy stem cell niches, where tumour prone cells are not activated. Ageing and pathological conditions may activate tumorigenic events. That tumour cells will arrange ECM in a different disposition that promotes hyperplasia and immune cells recruitment in tumour, which promotes cancer progression. Eventually, some cancer cells may enter circulation and reach another tissue. In that new location, they will induce ECM arrangements to promote new tumour creation. That process is known as metastasis. We can conclude that abnormal ECM niche arrangement induces tumour cell creation, proliferation and tumour cells extravasation (metastasis) (see Figure 2).

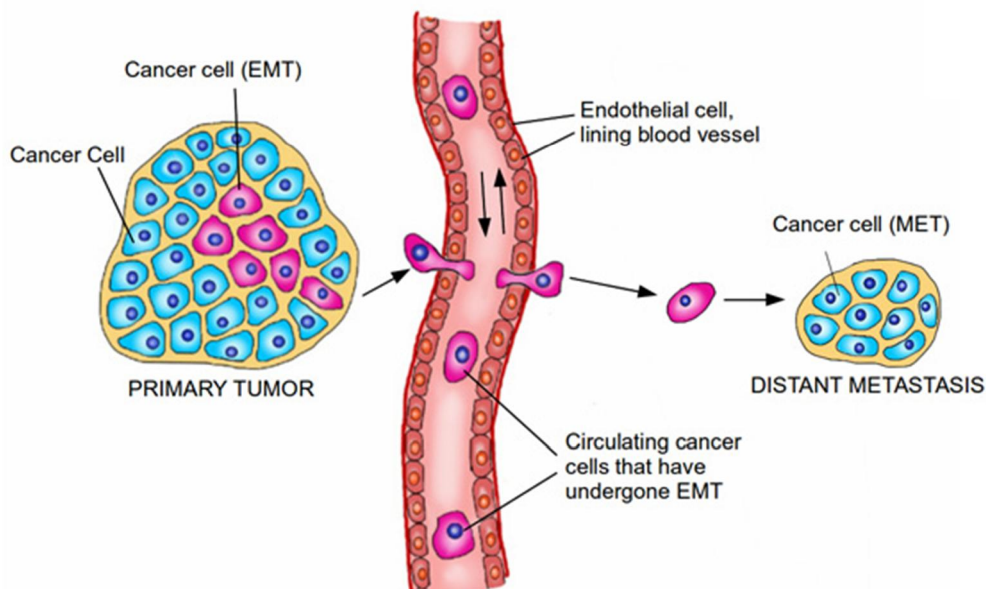


Figure 2 : Schematic representation of the basic mechanism of a metastasis process [8].

1.3 PROJECT BACKGROUND

The work developed in this bachelor thesis is part of a research project entitled “*Imaging and measuring cancer cell mechanics (CANCEL-*ME*)*” funded by the Spanish Ministry of Economy and Innovation with reference TEC2013-48552-C2-1-R. The project is coordinated by the Universidad Carlos III de Madrid (IP: Dr. Arrate Muñoz Barrutia). Other participating institutions are the Centro de Estudios e Investigaciones Técnicas (CEIT-IK4) leading a subproject (IP: Dr. Reyes Elizalde) and the Center for Applied Medical Research (CIMA) of the University of Navarra (leader Prof. Carlos Ortiz de Solórzano).

The main hypothesis of the project is that the carcinogenic transformation is a process in which the physical, cellular and molecular determinants react and adapt during the disease progression. The cancer invasion is initiated and maintained by signalling pathways that control cytoskeletal dynamics in tumour cells and by the connexions matrix-cell and cell-cell, followed by migration to the adjacent tissue. **The project plans to implement multidisciplinary approximations to obtain complementary, quantitative and multi-scale information about the initialization, the development and the treatment of cancer. Specifically, the project aims to study the mechanisms of the cell-matrix interaction and the remodelling process that happens during cell migration. Therefore, it is considered that the study of cell mechanobiology requires the development of tools to measure cellular forces in four dimensions (3D+time) within cellular environments that accurately simulate the cellular microenvironment.** Existing techniques are bidimensional and/or do not apply in realistic environments. Relevant information will be obtained through the viscoelastic characterization of the cancer cells (i.e., cytoskeleton) and the study of the changes in the mechanical properties experienced by the matrix during the tumoral dissemination.

The general objectives of the project are twofold, technological and scientific. One of the technological objectives is the development of *in vitro* assays with realistic and controllable properties re-enacting cell-matrix interactions and the cellular microenvironment. The second objective is the development of computation tools that allow a correct characterization of the mechanical properties of both the cells and the cellular environments. Another goal is to quantify the forces exerted by the cells into the matrix, all of that, in four dimensions (3D+time). Finally, the scientific aim consists in the application of the developed tools in the previous two points, to improve our knowledge about the mechanisms that govern cell-matrix interactions and the effect they have together with the microenvironment in the regulation of the cellular migration. In particular, distinctive elements between the behaviour of control cells (epithelial non tumoral) and of the tumoral cells (metastatic and non-metastatic) and the response to treatment will be identified.

The work was developed at the **Biomedical Imaging and Instrumentation Group (BiiG)** of the Biomedical Department of the Universidad Carlos III de Madrid, which is part of the Instituto de Investigación Sanitaria Gregorio Marañón.

BiiG is specialized in medical imaging, serving as a tool for the hospital investigators, but as well as a pioneer investigation centre in the development of new imaging tools, in terms of software and hardware. The BiiG laboratory space at the Hospital GU Gregorio Marañón contains PET (Positron Emission Tomography)/SPECT (Single Positron Emission Tomography) imaging machines, CT (Computed Tomography) scanners, MRI (Magnetic Resonance Imaging) and many other surgical and imaging tools. That material is used as a support for: clinical investigation performed in the hospital; preclinical investigations in mice; as a basis for technological imaging developments, both in hardware and software. The funding for the investigations usually comes from public money lines of investment but also from private assignments.

1.4 OBJECTIVES

The main objective of this bachelor thesis is to characterize the 3D network geometry of collagen hydrogels mimicking the extracellular matrix both in wells and micro-fluidic devices. Under the context of CANCEL-ME, culture wells will be the platform used in the experiments to estimate the tractions exerted by the cells on the matrix (known as Traction Force Microscopy). While the micro-fluidic devices will be the platform to study cell migration and the modification on it induced by therapy.

This general aim can be divided in the following particular objectives:

1. First of all, get a general idea of all the work involved from the lab work to the image acquisition. Hence, this objective can be divided into three sub-objectives:
 - 1.1 Learn how to prepare collagen hydrogels and how to place them in wells or in microfluidic devices.
 - 1.2 Understand how the microscopy images of these collagen hydrogels are taken and which acquisition parameters are tunable.
 - 1.3 Understand the implementation of the provided algorithms (FIRE, fibre extraction and pore size estimation) to characterize the 3D network geometry [2] [3].
2. Secondly, execute a study to confirm that FIRE is a reliable tool to extract the collagen network geometry. In that sense, two studies were performed:

- Generate artificial images of collagen networks using the simulator presented in [2] that will be used as ground truth to estimate the error made by FIRE.
 - Replicate the analysis described in [3] to get the code run and to work in parameter tuning.
3. The last objective to be mentioned is to use the FIRE program to analyse microscopy images taken from real collagen gels synthesized in the Instituto de Investigación Sanitaria Gregorio Marañón (IiGSM).

1.5 STATE OF THE ART

There exist biological evidences that the cells are affected by mechanical factors in processes like proliferation, migration and differentiation. The mechanical properties of the surrounding cellular environment are transduced to internal cell signalling pathways that regulate cell activities. The way by which cells translate the mechanical properties of their environment in specific genetic expression is called mechanotransduction, and it has become a recurrent topic for cell study since the early 00s because of its importance in cell fate. McBeath *et al.* demonstrated in 2004 that mechanical properties of the ECM induce signalling pathways that affect cytoskeleton reorganization, cell shape and lineages of differentiation in human mesenchymal stem cells [9].

The first time a fibre tracking algorithm was used for ECM characterization was in 2003, Wu *et al.* created a software for fibre extraction and used it to quantify collagen networks in prepared collagen hydrogels [10]. Stein *et al.* took that software and improved it with further processing steps and the possibility of calculating some fibre and network parameters [2].

Posteriorly, the final implementation of Stein *et al.*'s fibre extraction algorithm was used by Maska *et al.* to analyse collagen hydrogels' reflection microscopy images but with some pre-processing differences, like the use of steerable filtering instead of the Gaussian smoothing used by Stein *et al.* [3]. This pre-processing implementation is the one we are going to use for this project.

Moreover, there have arisen other papers that propose a collagen hydrogels pore size calculation from confocal images, based on medial axis computation algorithms [11] [12]. This last one is also incorporated in our analysis.

2.INTRODUCTION

In this chapter, the basic foundations of the experimental materials and methods used for this bachelor thesis will be presented focusing especially in the description of the collagen hydrogels and the reasons to use them; a brief explanation of the microfluidic devices and the basis of the microscopy techniques employed. It will be limited to the basic foundations of the experimental materials and methods used for this bachelor thesis.

2.1 COLLAGEN HYDROGELS

Collagen is a protein, main component of the extracellular matrix that forms all connective tissues in animals, so it is present in all the body [4]. Up to 35% of all the protein content in the body is collagen, the highest proportion in mammals.

Connective tissue is the one responsible to give support to the rest of the tissues in the body. It is mainly composed by extracellular material, the cellular content is very low and it is just covered by immune system cells and fibroblasts that are the ones who synthesize the extracellular components. Collagen is the most abundant and important of the extracellular components. It accounts for connective tissue supporting capacity, strength and elasticity, so it is considered to be the “glue” of the body tissues.

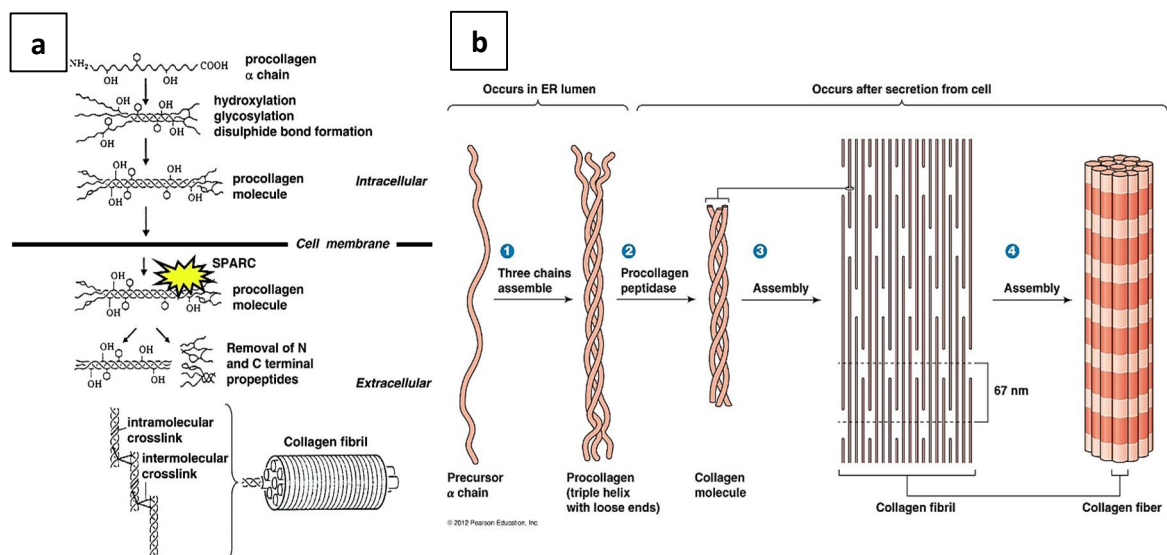


Figure 3: a) Collagen synthesis process [13]. b) Collagen structural arrangement [14].

As said before, collagen is synthesized by the fibroblasts in the form of procollagen, that it is expelled from the cell and transformed extracellularly in the final collagen molecules (see Figure 3a). The extracellular processing consists on N-end and C-end removal by N and C-proteinases. The procollagen and the final collagen molecules are structured in a triple helix. The final collagen triple helices are arranged to form collagen fibrils that at the same time are arranged to form the final collagen fibres (see Figure 3b).

Collagen has several subvariants depending on the type of tissue it is synthesized, leading to slightly different mechanical properties specifically needed for each tissue (see Table 1).

Collagen Type	Tissue Distribution	Cells of Origin
I	Loose and dense ordinary connective tissue; collagen fibres	Fibroblasts and reticular cells; smooth muscle cells
	Fibrocartilage	
	Bone	Osteoblast
	Dentin	Odontoblast
II	Hyaline and elastic cartilage	Chondrocytes
	Vitreous body of the eye	Retinal cells
III	Loose connective tissue; reticular fibres	Fibroblasts and reticular cells
	Papillary layer of dermis	
	Blood vessels	Smooth muscle cells; endothelial cells
IV	Basement membranes	Epithelial and endothelial cells
	Lens capsule of the eye	Lens fibre
V	Fetal membranes; placenta	Fibroblasts
	Basement membranes	
	Bone	
	Smooth muscle	Smooth muscle cells
VI	Connective tissue	Fibroblasts
VII	Epithelial basement membranes; anchoring fibrils	Fibroblasts and keratinocytes
VII	Cornea	Corneal fibroblasts
IX	Cartilage	
X	Hypertrophic cartilage	
XI	Cartilage	
XII	Papillary dermis	Fibroblasts
XIV (undulin)	Reticular dermis	Fibroblasts
XVII	P170 bullous pemphigoid antigen	Keratinocytes

Table 1: For each collagen type, the tissues in which they are present and the cells of origin are listed [4].

Collagen is used for therapeutic and research purposes like for instance as drug delivery scaffold or for cosmetic surgery. Hence, it is widely produced by genetically engineered organisms and commercialized.

Hydrogels are three dimensional structures made of a polymer backbone and a high amount of water inside, as the polymer usually contains many hydrophilic groups [15]. They result from the crosslinking of a polymer in specific conditions. The applications of hydrogels are wide, especially in tissue engineering as they resemble the consistency of the extracellular matrix and can be made of extracellular protein components. Collagen hydrogels are good ECM substitutes or models as collagen is the most abundant protein in ECM.

2.2 MICROFLUIDIC DEVICES

Microfluidic devices are small sized systems that can manage very small volumes inside their micro-scale sized channels [16]. The main advantage of these devices relies on the control of the input of substances that channels receive and take advantage of the micro properties of the system. They are usually used for culturing cells, as the variability under which cells are becomes highly controlled.

The majority of these devices are made of polydimethylsiloxane (PDMS), which is an organic polymer based on silicon. PDMS is so interesting thanks to its properties: Any kind of pattern can be imprinted in it through microfabrication techniques; it is cheap and easy to manufacture; its transparency facilitates observation of the microfluidic device under the microscope.

Those reasons above make PDMS microfluidic devices really helpful in terms of growing cells in a controlled medium, where any fluxes can be introduced and chemical, mechanical or biological inputs can be set to study the cell behaviour.

2.3 REFLECTION AND CONFOCAL MICROSCOPY

2.3.1 REFLECTION MICROSCOPY

Reflection microscopy is an optical microscopy technique that is based on the reflections that an incident beam of polarized light suffers when crossing different materials, each one with its specific refractive index [17]. The sample to be observed

has to be placed on a glass surface. This microscopy technique is usually used to visualize cells, but the high resolution and high contrast allows to see the collagen fibres as well although they are on the range of 10 micrometres.

The theoretical principle in which reflection microscopy is based is the following: Light with a known wavelength passes through a polarizer, filter that removes all the possible polarizations of light beam, except of one. The polarized beam goes then to a beam splitter and it is reflected in the objective, which focuses the beam on the bottom (glass) of the sample. Light crosses the sample and can be reflected at different indexes either by the glass or by the sample components. The light reflected comes back to the beam splitter and then to a second polarizer that is in charge of eliminating light scattering. Finally, the reflected polarized light reaches a CCD camera detector that creates the image of the sample (see Figure 4).

This image technique is quite simple as it just needs a light source some filters and a detector, so it is cheap and rapid to implement.

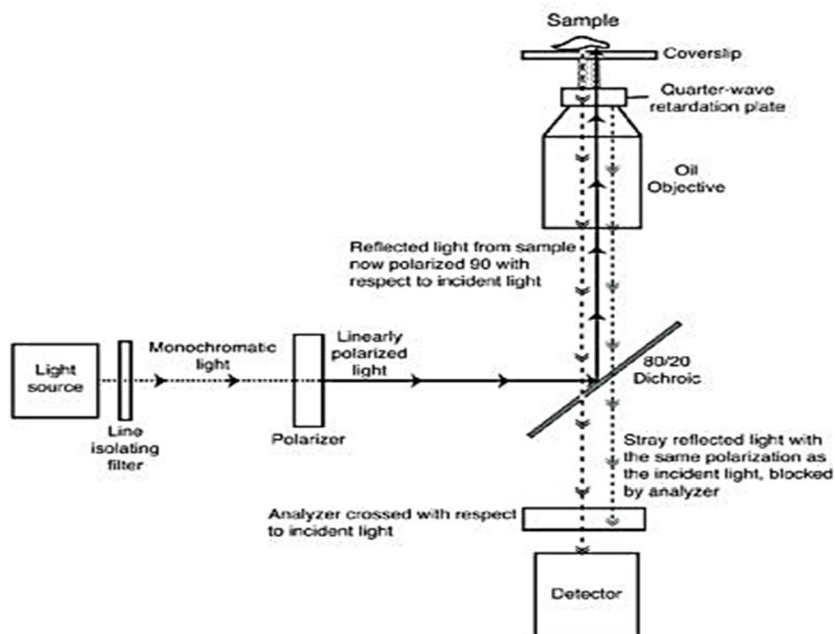


Figure 4: Reflection microscopy set up [17].

2.3.2 CONFOCAL MICROSCOPY

Confocal microscopy is an optical imaging technique that improves the contrast of the image by eliminating the light that produces blurring in the image (see Figure 5) [18].

In standard optical microscopy, the areas that are out of the focal plane still contribute to the image by adding out of focus blur. However, in confocal microscopy, the addition of a spatial pinhole between the sample and the detector eliminates the out

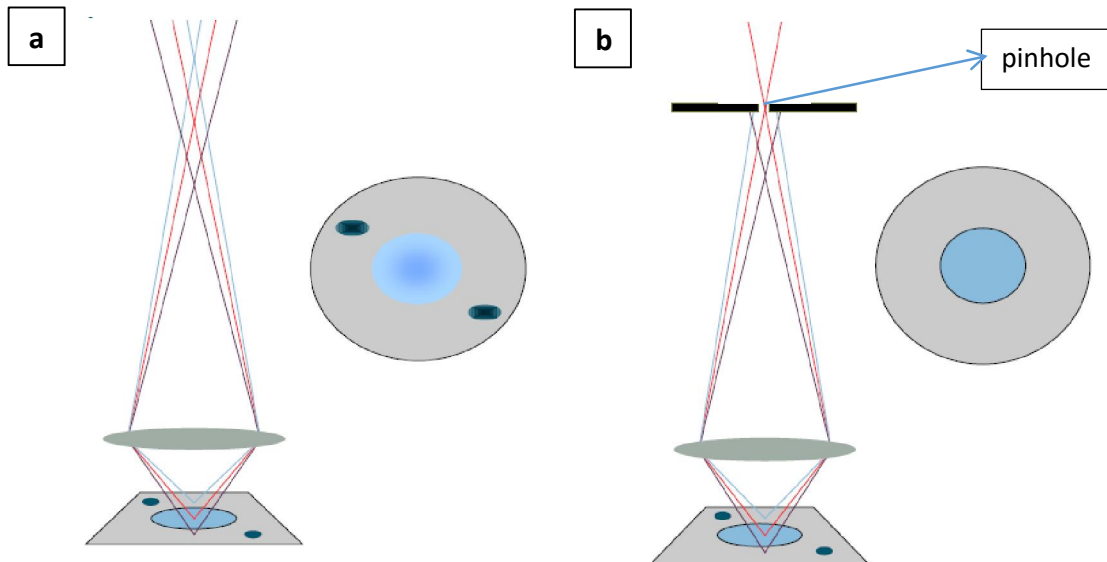


Figure 5: a) Reflection microscopy of sample: blurring in the final image. b) Confocal microscopy: pinhole used, selecting information retrieved [19].

of focus reflected light that produces the blurring (see Figure 6). That feature permits to receive only the desired light range, selecting thus only the information corresponding to a single focal plane. Taking several slices at different focal levels allows reconstructing a 3D view of the sample with more contrast than in simple reflection microscopy. Apart from increase in contrast, another important feature that confocal microscopy offers is that depth of the field can be controlled. Confocal microscopes can be used in reflection mode and in fluorescence mode.

The main drawback of confocal fluorescence microscopy is that the sample has to be first labelled with a fluorescent dye, which is an expensive and laborious process.

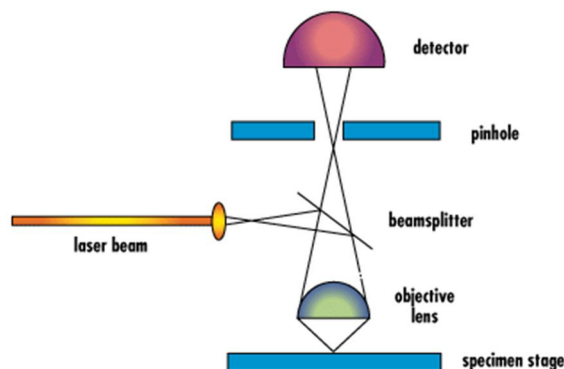


Figure 6: Confocal microscopy set up with basic components [20].

To sum up, simple reflection microscopy is immediate and fast but it drags the blurring problem. At the same time, confocal solves that blurring problem and increases the contrast but in the case of fluorescence, it requires a more extended and costly pre-processing of the sample.

3. MATERIALS AND METHODS

This chapter describes the collagen hydrogel image sources available for the project plus all the experimental and computational steps followed in order to develop the study of network extraction and characterization of collagen hydrogels images.

This chapter is structured following the order of steps performed in the experiment, that is, Section 3.1 explains the main network parameters to study. Sections 3.2 to 3.4 describes the three types of collagen hydrogel images used and how are they obtained. Section 3.5. describes the image processing pipeline followed to binarize the images. Finally, Section 3.6. presents the algorithms used for the network extraction and the characterization of the collagen hydrogel images.

3.1 COLLAGEN NETWORK'S PARAMETERS OF INTEREST

The most important parameters to characterize the collagen networks in the context of the present bachelor thesis are:

- **Fibre Length:** The length of each fibre is determined taking into account the resolution of the image in the three axes (introduced as an input parameter) [2].
- **Fibre Persistence Length:** Persistence length is a measurement of the stiffness of a polymer [21]. The pieces of polymer that are shorter than the persistence length are mechanically flexible while longer fibres' mechanical properties can only be defined statistically. The formula used for computing the persistence length of a polymer chain is [2]:

$$\cos(\theta(l + \Delta l) - \theta(l)) = e^{-\frac{\Delta l}{Lp}}$$

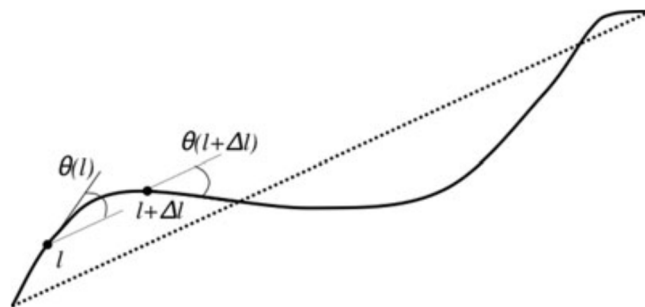


Figure 7: Persistence length basis [2]

This fibre persistence length computation is based on following a fibre persistent random walk, computing persistence length for each fibre section. The tangent angle (θ) to the fibre changes as the fibre grows and changes direction, and the basis for updating that tangent angle is based on persistence length definition. l is the length from the fibre origin to the start point of a fibre segment while $l + \Delta l$ is the length from the fibre origin to the end point of the segment. L_p the persistence length (see Figure 7).

- **Pore Size:** The size of the pores of the fluid phase between the fibres is defined as the average radius of the spheres filling the fluid phase spaces [11].
- **Crosslink Density:** It is defined as the length density of crosslink points in the fibre network [2]. A cross-link is a bound that links one polymer chain to another.

$$D_c = \frac{N_c}{L_T}$$

with D_c as the crosslink density per unit length, N_c as the total number of crosslinks in the network and L_T as the total length of the fibres of the network.

3.2 ARTIFICIAL IMAGES

A simulator was used in order to create three dimensional artificial collagen network's images, so as to test the performance of the fibre extraction algorithm.

The simulator is a set of functions written in MATLAB created by Andrew Stein as part of the fibre extraction algorithm package (FIRE). It is available for free download at the webpage: <http://www.andyste.in/software>.

This simulator permits the user to rigorously control what images are created and the exact tuning of the main ruling parameters of interest. They are:

- The **size of the images** in the three axes, both in pixels and in micrometres.
- The pixel size** of the image in the three axes.
- The hydrogel collagen fibre network density and the collagen density of the stock collagen solution.**
- The **fibre diameter**

-The **fibre length distribution** → This fibre length is based on an exponential distribution of fibre lengths, with a mean of 10.4 micrometres.

-**Fibre persistence length distribution** → The persistence length of each fibre can be set manually but, as in fibre length, the default computation assignment is simpler. That computation is based on persistence length calculation explained in Section 3.1.

- **The standard deviation of the Gaussian smoothing:** Gaussian smoothing is used to make the image more realistic than the output binary image by adding blur.

- The **parameter to modulate the amount of noise** added to the image.

-The **Z-step**→ Parameter that determines the factor of resolution reduction in the z-axis. This functionality may be interesting to be added since resolution of collagen hydrogel's images in the z-axis is usually lower.

The steps that the program implements in its workflow are:

1.- The number of fibres for the network image volume is computed from the input parameters using a formula extracted from experimental data results:

$$A = \pi r^2$$
$$K = D_s \cdot A \cdot 10^4$$
$$N_F = \left[\frac{D_g \cdot K}{W^3} \right]$$

Being D_g the density of the collagen hydrogel for the image, D_s the concentration of the collagen stock solution, W the pixel width of the artificial image and r the radius of the fibres.

2.- For each fibre, a length of the exponential distribution is assigned, and the corresponding persistence length is computed.

All the input parameters and the length information computed for each fibre are stored in a MATLAB structure so as to have it available.

3.- A three-dimensional volume of zeroes, with the sizes specified, is created. Afterwards, each fibre is printed as a line of ones in a random position and orientation, but preserving the length and persistence length assigned for the fibre.

4.- A Gaussian smoothing operation is applied to calculated fibres in order to get a more realistic image (see Figure 8).

5.- The z-axis of the image is reduced in pixels by a factor of the value of zstep. This step is performed because the resolution in z-axis of confocal images is usually lower than in x-axis and y-axis.

6.- Random salt and pepper noise is added to the image if desired. The amount of noise addition is modulated by an input parameter as explained before.

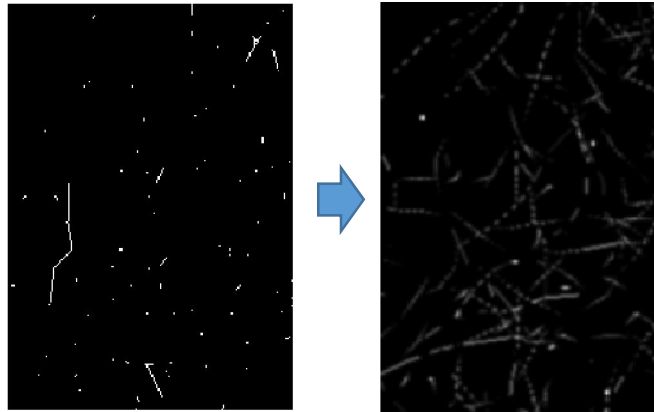


Figure 8: Step from binary artificial image to Gaussian smoothed artificial image.

Artificial binary images at 1/1.5/2/2.5 gel density were created in order to test FIRE. Twelve images volumes were produced with the following input specifications:

- Pixel size of 0.225 μm /pixel in the three axes.
- 315x315x315 spatial resolution.
- 0.075 μm of fibre diameter.
- Exponential distribution of fibre lengths.
- Gaussian smoothing and noise addition were not performed as not to modify the selected parameters for the network structure.

3.3 PREVIOUS LITERATURE IMAGES

The collagen network images acquired for [3] were kindly provided by Prof. Carlos Ortiz de Solórzano from CIMA – University of Navarra. As previously indicated, we use those images to tune the pipeline parameters and study the reproducibility of the results.

This material consists of confocal reflection images of three types of collagen hydrogels, each one with a specific proportion of collagen and Matrigel:

- **Dataset I:** Only collagen (at 2 mg/ml)
- **Dataset II:** Collagen and Matrigel at 1:1 proportion, both at 2 mg/ml.
- **Dataset III:** Collagen and Matrigel at 1.2 and 4 mg/ml respectively.

Matrigel is synthesized by mouse sarcoma cells, and it is composed mainly by laminin, collagen IV, heparin sulfate proteoglycans and growth factors [22]. That composition is, along with collagen type I, similar to the extracellular matrix composition. Consequently, it is theoretically very useful to add Matrigel to collagen hydrogels for the full emulation of ECM.

Twelve image volumes were taken at confocal reflection microscopy for each Dataset, with 512x512x30 spatial resolution for the three axes, and 0.279x0.279x0.43 μm of pixel size in each axis (see Figure 9). The microscope and objective used were Zeiss LSM 510 confocal microscope equipped with an oil-immersion Plan-Apo 63x/1.4 objective lens.

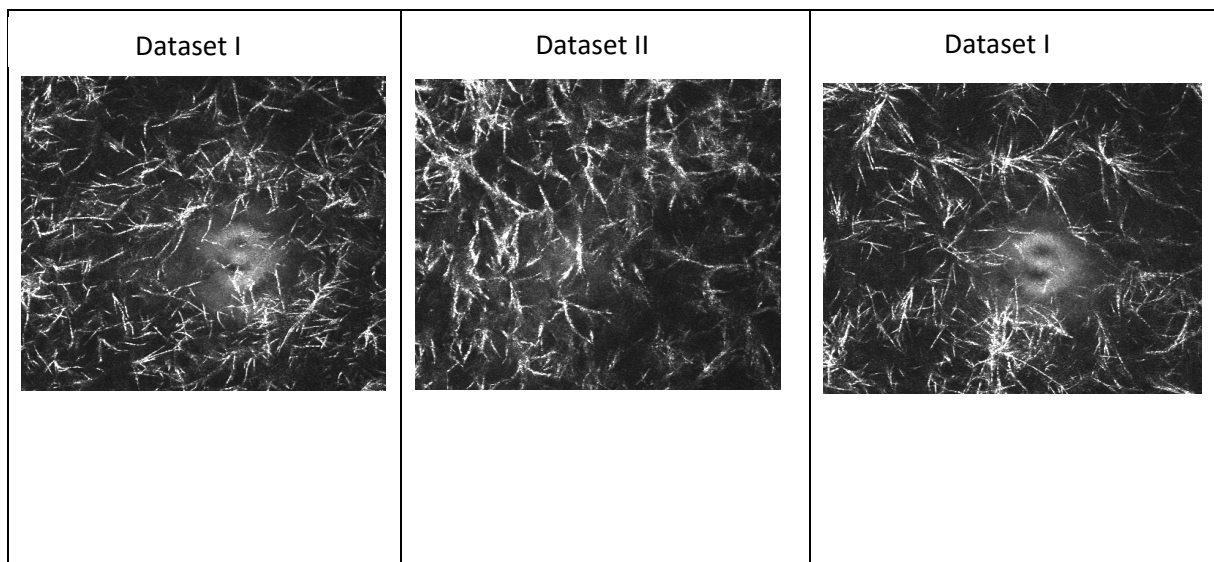


Figure 9: Image examples for Dataset I, II and III, from left to right..

3.4 OWN REAL IMAGES

In this section, the main steps gone through in order to obtain our own real collagen hydrogel images will be explained.

3.4.1 COLLAGEN HYDROGELS PREPARATION

Gels at different concentrations were prepared at the laboratories of the Unidad de Medicina and Cirugía Experimental (UMCE) of the Hospital GU Gregorio Marañón. The experimental work was performed by Mario Arjona, a chemist that works as Research Assistant at BiiG.

The concentrations chosen for collagen gels were: 1 mg/ml, 1.5 mg/ml, 2 mg/ml and 2.5 mg/ml.

The reactants and materials used were the following:

- Collagen type I rat tail (stock at: 3.43 mg/ml)
- Phosphate Buffered Saline (PBS) (10X)
- Distilled water
- Sodium Hydroxide (NaOH) 0.5 M
- Culture plate with eight wells and glass bottom

The procedure, based on previous studies [3], was the following:

1. First, we have to ensure that all reactants are kept at around 4^o Celsius throughout all the process, using a recipient with dry ice that avoids the sudden polymerization of collagen.
2. The volume of the stock collagen concentration that is necessary to reach gel concentration is extracted, taking into account the concentration indicated in the collagen stock canister.
3. Table 2 below describes the exact volume of H₂O, NaOH and PBS 10x necessary to neutralize the collagen for each different concentration. Mix them gently into a 1.5 ml Eppendorf Tube before the next step.
4. The neutralization solution and the collagen volume extracted from stock solution are gently mixed, making sure that the final solution is homogeneous.
5. 300 µl of the final solution are introduced in each well and microfluidic device, trying to avoid bubbles.

6. The well plates and the microfluidic devices are incubated at 37° Celsius and 5% of CO₂ for 90 minutes.

The most critical part of the hydrogel preparation is the neutralization process of the original PH 2 collagen solution. It is crucial to reach a physiological pH, in the range of 7-7.5, to ensure a good polymerization of collagen fibres. For that purpose, pH test strips are used to ascertain that the pH of the water/sodium hydroxide/PBS mixture is in the range of 4-5. At the same time, final collagen solution for hydrogel formation must be checked as well to get the range of 7-7.5.

As previously referenced, Table 2 shown below contains the final adjusted volumes of reactants. The final volume is 300 µl having the four different final collagen concentrations prepared in this work:

Reagent/Concentration	1 mg/ml	1.5 mg/ml	2 mg/ml	2.5 mg/ml
Collagen (µl)	87.465	131.19	192	218.655
PBS 10X (µl)	83.76	61.92	30	21.12
H ₂ O (µl)	121.26	99.42	67.5	58.62
NaOH (µl)	4.5	5.25	7.5	9
Total (µl)	296.985	297.78	297	307.395

Table 2: Volume of reagents needed for preparing each concentration, starting from a 3.43 mg/ml collagen I rat tail stock at pH=2.

3.4.1.1 FLUORESCENT COLLAGEN HYDROGELS

The collagen hydrogel preparation explained previously can only be observed under reflection microscopy. Getting images of collagen fibres with fluorescent confocal microscopy needs of fluorescent stained fibres preparation. Fluorescent collagen fibres were prepared by labelling them with red-fluorescent tetramethylrhodamine (TAMRA). TAMRA is a fluorophore that dyes molecules with fluorescence so they can be easily identified with confocal fluorescence microscopy.

3.4.2 WELLS AND MICROFLUIDIC DEVICES

Once the Collagen Hydrogels at different concentrations are prepared at 4°C, they are lead to polymerization at 37°C. The first in vitro platform for that were **culture wells**.

They allow imaging the hydrogel under the microscope as they are made of transparent material (see Figure 10).



Figure 10 : Wells culture plate used

However, the aims of this project is to eventually introduce cells in these collagen hydrogels simulating the ECM and study the ECM-cell interactions in **controlled conditions**. Consequently, one of the main objectives is the study of how far **microfluidic devices** are useful as a highly controlled platform to develop 3D cell culture studies

The microfluidic device option used for the experiment was based on the design described in Shin *et al.* paper [23]. In Figure 11, it is shown the design of the microfluidic device. It is composed by a central chamber, connected to two auxiliary lateral channels used for hydrogel and cell culture insertion in the microfluidics device. In order to keep the hydrogel and the cells inside the central chamber, a system of posts along the interconnections between the central chamber and the lateral channels was designed.



Figure 11: a) Microfluidic device sketch. b) Real microfluidic device [23].

The procedure of fabrication relies on the replica-molding manufacturing, a master is created and then replicated (see Figure 12). The summary of the steps to follow is:

1. **Photolithography:** Fabrication of the master mold on silicon wafers by means of spin-coating a UV photoresist to the surface of the wafer. The photoresist used is SU-8, a substance that crosslinks when exposed to UV radiation. A mask that leaves open to radiation the desired geometry to crosslink is placed on top of the photoresist coating. UV light is applied, so that the parts that are not coated by the mask remain unmodified and can be washed afterwards, while the parts that are affected by UV suffer crosslinking. That creates the desired pattern to be transformed in PDMS.
2. **Soft lithography:** Once the pattern mold master is created on the silicon wafer, PDMS is poured on it, along with a curing agents solution. The wafer is then cured for 48 hours at room temperature. Afterwards the PDMS is cut to separate the individual chips, and the holes designed for the introduction of the gels or solutions into channels are created by using dermal biopsy punches of different diameters.

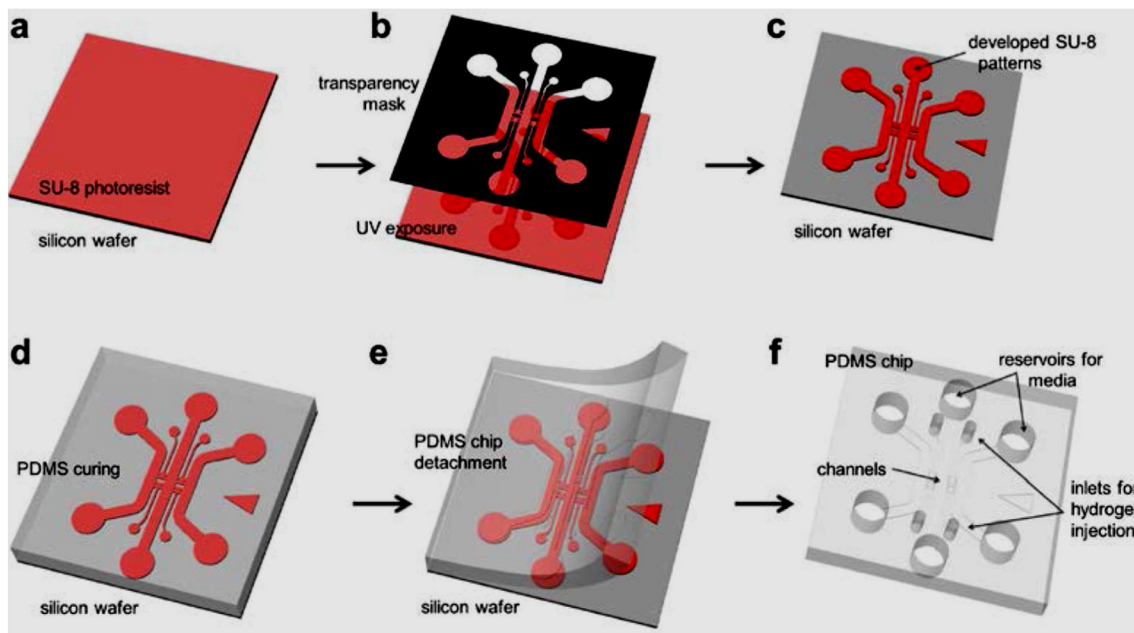


Figure 12: Microfluidic devices production in PDMS [23]: a) Photoresist film addition. b) Mask addition c) UV light applied. d) PDMS curing. e) PDMS removal. f) Inlet channels creation.

After the microfluidic device is created, it is covered with Poly-D-lysine to enhance attachment of cells. However, this step was not implemented as the goal of this project was just testing collagen hydrogels separately. The collagen solution is

introduced with a micropipette in the central chamber through the inlets of the microfluidics device.

Finally, the microfluidics device is placed on a Petri dish with the bottom covered by water and introduced in an incubator at 37 degrees Celsius and 5% of CO₂ for at least 30 minutes in order to produce collagen fibres polymerization.

Microfluidic devices are a potential useful platform for collagen network characterization, especially when introducing cells as well, since they offer a cheap, reproducible and controlled environment for cellular study. Transparency of PDMS allows as well the possibility of taking microscopy images of the device in order to trace cell behaviour and proliferation.

3.4.3. MICROSCOPY IMAGE ACQUISITION

In order to evaluate the difference in image quality within the real images of collagen hydrogels, the idea is to use both reflection and fluorescence confocal microscopy imaging techniques explained previously and hence choose the best option based on the results.

Real images from Collagen Hydrogels at different concentrations were acquired in both wells and microfluidic devices with the use of reflection and fluorescence confocal microscopy.

Before acquiring the images with the microscope, the samples contained into the two different in vitro platforms were prepared. Once the collagen hydrogels were polymerized, they were fixated to avoid the rupture of the fibre network and to keep it intact for a long period of time. The fixation procedure is performed by adding formaldehyde at 5% for 5 minutes. Then, formaldehyde is removed and PBS added to avoid gel dryness.

Twelve image volumes at the four collagen hydrogel concentrations prepared (1/1.5/2/2.5 mg/ml), both for culture wells and microfluidic devices, were acquired with a Leica SP2 confocal microscope. The non-fluorescent preparations were acquired in a reflection microscopy mode and the fluorescent collagen hydrogels with a confocal fluorescent microscope. The images were acquired by Dr. Rafael Samaniego, the head of the confocal microscopy unit at UMCE of the Hospital GU Gregorio Marañón.

For both microscopy modes, the laser emission wavelength was 479 nm, which corresponds to red emission spectrum. The pinhole used was of 0.247 mm. A glycerol immersion objective with a magnification of 63X and a Numerical Aperture of 1.3 was used.

The images taken are set to have a pixel size of 0.232 micrometres in x and y direction and of 0.41 ± 0.02 in z-axis. The dimensions of the images were 1024x1024x30 pixels, so the field of view is 238x238x13 micrometres (see table 3). The pixel size in z-axis was set to 0.41 ± 0.02 in order to fulfil the Nyquist theorem avoiding the loss of information in the axial direction. The bit depth was 16.

Axis	Pixel size ($\mu\text{m}/\text{pixel}$)	Dimensions(in pixels)	FOV(μm)
X	0.232	1024	238
Y	0.232	1024	238
Z	0.43	30	13

Table 3: Real images acquisition parameters

The aim was to reach up to 12 image volumes with those specifications for each of the four concentrations, for hydrogels prepared into wells and microfluidic devices, similarly to the image stacks used in *Martin et al.* [3] (see Figure 13 and 14).

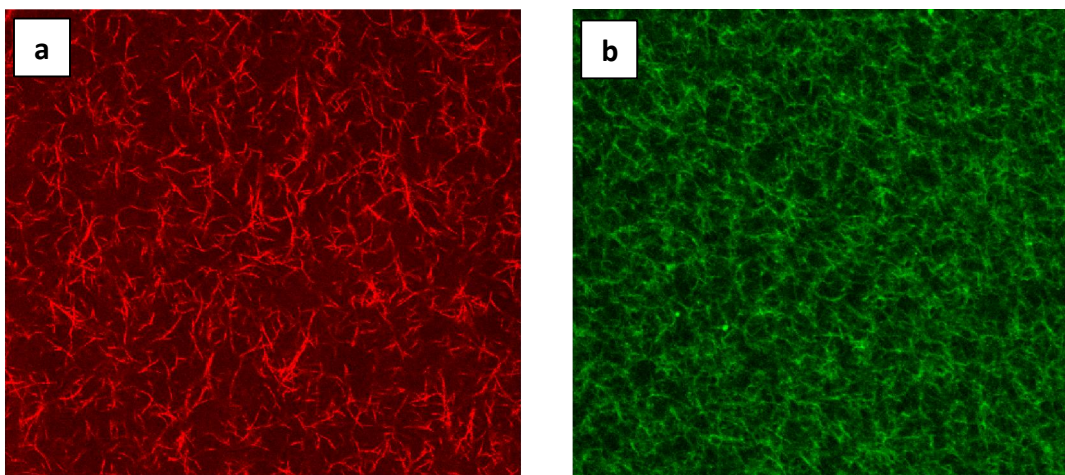


Figure 13: Sample images of collagen hydrogels with a concentration of 1.5 mg/ml polymerized in wells: a) Reflection Microscopy. b) Confocal microscopy

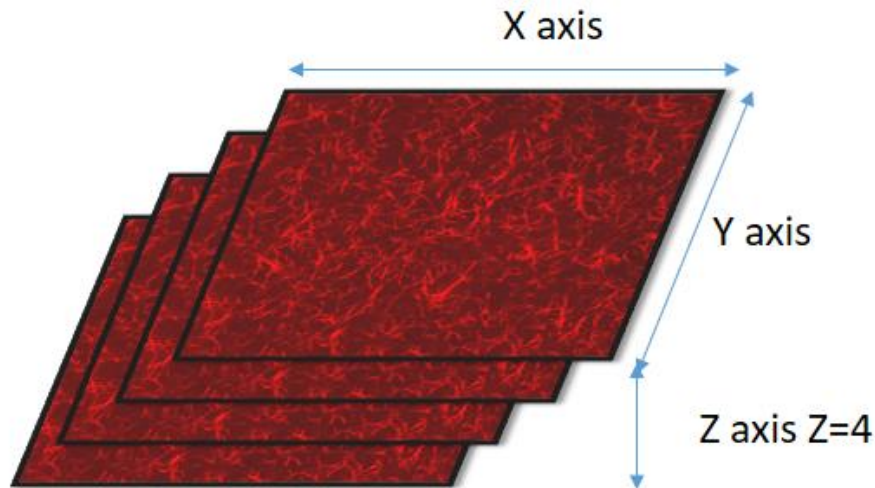


Figure 14: Schematic representation of real collagen hydrogels images (stack of 4 images).

3.5 IMAGE PROCESSING PIPELINE

Having in mind the final goal of extracting the network geometry of the collagen gels, after image acquisition, the binarized network mesh need to be computed, as it is a required input for the FIRE software. The image processing pipeline was the one described in Maska *et al.* [3]. The main steps were: 1) Fibre enhancement and noise reduction using a steerable filtering; 2) Binarization by an Otsu threshold.

3.5.1 STEERABLE FILTERING

Filtering is a key step in the implementation of any kind of image processing. Images are usually affected by different types of noise that reduce the final quality of the image. Hence, noise elimination is primordial in order to get enhanced images for their visualization and corresponding processing.

In this work, collagen hydrogel's images contained a high amount of background noise especially due to free non-polymerized collagen monomers and too shortly polymerized fibres.

To overcome that problem, filtering before binarization is applied on the image, otherwise all the background noise pixels would be included inside the threshold as if they were part of fibres, and thus the binarization would not separate fibres from background.

There are many types of filters that can be used; however, steerable filters are well-known for their ability to enhance fibre-like structures and reduce noise.

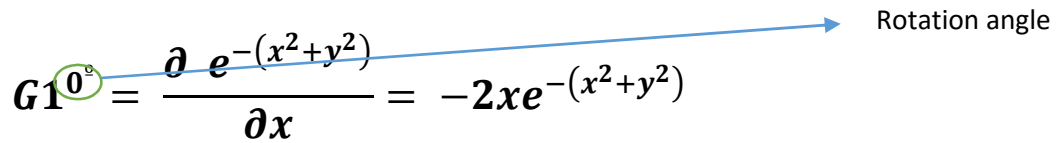
-Steerable filtering

Steerable filter implementation is based on oriented filtering. That seems to be very useful because this filter finds the specific orientation of each fibre in the 3D space and filters them according to their direction. In order to build a steerable filter that responds to the orientation of the image features, the best option is to apply a few variations of the same filter, each one with a different angle of rotation (orientation) and then interpolate the filter responses [24]. Therefore, it is possible to filter along the correct directions without directly applying a filter in a specific orientation. This feature becomes vital for the project images, as each fibre has a different orientation.

The most representative and used case for steerable filtering is the linear combination of Gaussian derivatives. Considering the 2D Gaussian function:

$$G(x, y) = e^{-(x^2+y^2)}$$

The first x derivative of the Gaussian is:

$$G1^{0^\circ} = \frac{\partial e^{-(x^2+y^2)}}{\partial x} = -2xe^{-(x^2+y^2)}$$


The same function rotated 90 degrees is equal to the first derivative in y of the Gaussian:

$$G1^{90^\circ} = \frac{\partial e^{-(x^2+y^2)}}{\partial y} = -2ye^{-(x^2+y^2)}$$

Interpolation of that Gaussian filter for any angle θ as a linear combination of these two oriented filters is hence:

$$G1^\theta = \cos(\theta)G1^{0^\circ} + \sin(\theta)G1^{90^\circ}$$

$G1^\theta$ represents a steerable filter of first order (see Figure 15 a, b and c). Nevertheless, for this project a second order steerable filter is used, made of second derivatives of the Gaussian. The main advantage of second order steerable filter is the fact that it is able to enhance each fibre in its particular orientation (see Figure 15 d and e).

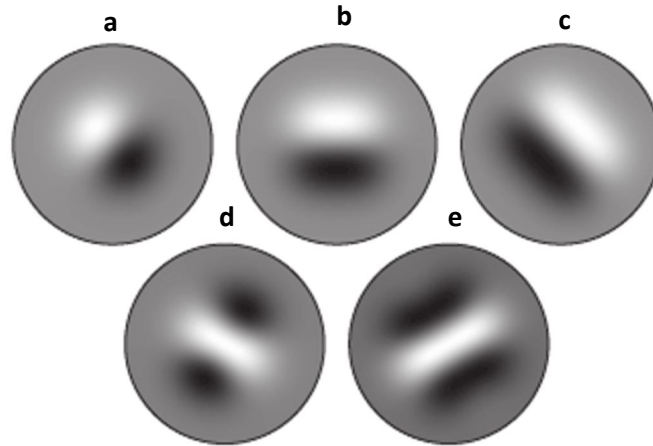


Figure 15: Examples of steerable filters masks for feature detection: *a*, *b* and *c* masks correspond to Gaussian steerable filters of first order; *d* and *e* masks correspond to Gaussian steerable filters of second order [25].

The function that calculates the steerable filter for this work was implemented in C++ by Martin Maska as part of his work on collagen networks characterization [3]. It uses second-order derivatives of the 3D Gaussian function as basis for the steerable filtering. This program only requires as inputs the image to be filtered, the pixel size in each axis and the standard deviation of the Gaussian filter in each spatial direction.

3.5.2 IMAGE THRESHOLDING

After noise removal, fibres can be separated from background and binarized using an Otsu thresholding.

Otsu thresholding is based on minimizing the within-class variance, which is the same as maximizing the between-class variance [26]. That means that the value of the pixels in each threshold range has to be as similar as possible. The threshold value is computed directly from the gray-value histogram of the image. The computational implementation is based on computing the between-class variance for each possible threshold, and determine for which threshold the between-class variance is maximum.

All pixels whose value is higher than the threshold computed will be set to 1 (white), which are supposed to be fibre pixels, while those ones whose value is lower than the threshold will be set to 0 (black/background pixels).

This type of thresholding is especially useful when the image histogram is bimodal, that means that there are two or more differentiated histogram peaks that will be separated by the thresholds. Thus, the separation of the two or more different image features is achieved.

In Figure 16, a sample histogram of a collagen hydrogel and the corresponding Otsu threshold are shown.

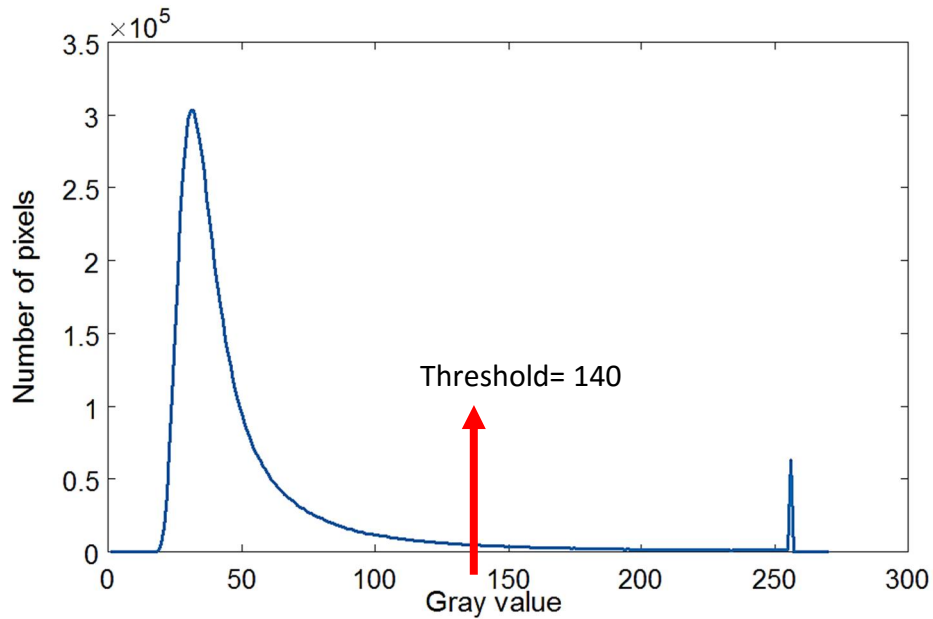


Figure 16: Collagen hydrogel image histogram with its Otsu threshold for binarization.

The optimal performance of our binarization is especially affected by the ability of the steerable filter used to remove noise efficiently and preserve the fibres.

3.6 QUANTIFICATION OF 3D NETWORK GEOMETRY

In this section, the main steps that this particular algorithm follows in order to extract the fibre network geometry of a collagen hydrogel three-dimensional image will be explained.

The algorithm used for 3D fibre network extraction from microscopy images is called FIRE (**FibeR** Extraction) and was implemented in MATLAB by Stein *et al.* [2].

The inputs required by FIRE are: The binarized three dimensional image and some other key parameters ruling the computation performed by the software

From Section 3.6.1 to 3.6.6, all the crucial steps performed during fibre network analysis made by FIRE are summarized. Pore Size calculation is explained in Section 3.6.7.

3.6.1 DISTANCE FUNCTION

The input binarized image of the collagen network is firstly transformed into a distance function image. This step is implemented by using the MATLAB function *'bwdist.m'*, that substitutes each white pixel by the minimal distance from this pixel to a black one (background).

Afterwards, the distance function is smoothed with a Gaussian filter of standard deviation equal to one, as that seems to improve the overall fibre extraction process [2].

3.6.2 NUCLEATION POINTS FINDING

A **Nucleation Point (NP)** is defined as local maxima of the image's distance function. The program that extracts the nucleation points in the image is called *'findlocmax.m'* and it localizes the local maxima in the smoothed distance function. The image is divided in cubic sub-images of dimensions specified in the input parameter structure (S_{xbox}). Inside each cubic sub-image, the pixel whose value is maximum is defined as nucleation point if its value is higher than a threshold specified by the user (Θ_{nuc}). Nucleation points that are closer than 2 pixels to each other in the image are fused to just one.

3.6.3 FIBER EXTENSION

As the nucleation points locally maximize the distance to the background, extending nucleation points towards their neighbourhood maximums will result in the identification of the image's fibres.

Nucleation points' extension is performed by the FIRE's routine called *'extend_xlink.m'* and it is illustrated in Figure 17. The program takes the smoothed distance function image and the list of nucleation points' position. One by one, **the local maxima** (LMPs) surrounding each nucleation point are localized. LMPs can only be maxima of the NP's surrounding box (set as LMP searching space). These surrounding maxima cannot be lower than a threshold Θ_{LMP} (input parameter).

-The most common situation is a NP that holds two LMPs, which have to keep an angle close to 180 degrees, as these are the two directions for fibre extension.

The coordinates of all the points that form part of any fibre are stored so as to have available the information for each fibre in the network, allowing network parameters computation plus the option to print the network.

The program that interpolates from NPs and LMPs to fibres expressed in coordinates is called '*fiberproc.m*' (part of FIRE package).

3.6.5 FIBER PARAMETERS COMPUTATION

Once the network of collagen fibres has been extracted, FIRE's routine '*network_stat.m*' computes some structural parameters (i.e., fibre length, fibre persistence length, crosslink density).

3.5.6 BEAM NETWORK FORMATION

It is possible to visualize the network extracted by FIRE plotting the 'skeleton' made of fibres that conform the whole network. Furthermore, this visualization is made more realistic by transforming the one-pixel thickness fibres to cylindrical beams. The routine that performs that task is inside FIRE package, and it is called '*beamproc.m*'.

By the end of this processing part, all the information about fibre processing, the results on fibre network extraction and all the parameters of the network computed are stored in a MATLAB structure.

3.6.7 PORE SIZE COMPUTATION

Pore size is one of the most critical parameters to be controlled in our collagen hydrogel network, as it has been shown to affect the behaviour of the cells. Pore size has been demonstrated to determine the migration pattern of some cell types as cancer cells, fibroblasts or inflammatory cells through a hydrogel [11].

Pore size can be computed directly from a binarized version of a collagen hydrogel microscopy image, which means **it is independent from FIRE algorithm**. Several methods can be implemented but covering radius transform-based computation is the most effective [11].

-Covering radius transform pore size computation

This method is based on a separation of the fluid phase of the binarized image (background=black pixels or Zero value pixels) from the solid phase (fibres = white pixels or 1 value pixels). The width of the collagen fibres is reduced so as to keep the fibres as just lines of one-pixel width. These lines of white pixels are the medial axis of the fibres. The pore size distribution of the network is set to be the distribution of the covering radius transforms. For each voxel v of the image, the covering radius transform assigns it a value Df , that is equal to the radius of the largest sphere with centre anywhere in fluid phase that covers the voxel v .



Figure 18: Covering radius transform spheres in the fluid phase [11] .

Pore size can be defined as the average of covering radius transform, since the spheres fill the fluid phase. The covering radius pore size distribution $p(r)$ is then normalized to the final volume of the fluid phase (V_f):

$$\int_{r=0}^{\infty} p(r) dr = V_f$$

Another pore size distribution can be obtained by just considering those spheres that lie in the medial axis of the fluid phase (see Figure 18). This distribution is normalized to the union of volumes of medial axis spheres instead to the total fluid phase volume.

The algorithm used for computing the pore size of collagen hydrogel images was implemented by Martin Maska in C++ as part of his work in collagen networks characterization, and it is called 'i3d_crt.mexw64' [3]. This algorithm requires as inputs the information for each fibre coordinates resulting from the FIRE processing, plus the

resolution of the image. First, it reconstructs the fibre network image from that information about the fibres. Afterwards, the pore size is computed based on medial axis covering radius transform distribution method. The output is the mean value of the pore size distribution of our network.

4. RESULTS

This chapter includes all the collagen hydrogel's images analysis performed using the processing pipeline proposed which is based on binarization and fibre extraction (FIRE algorithm). FIRE algorithm parameters values used for all analysis are specified in Annex I.

Section 4.1 describes the evaluation of the software pipeline using synthetic images. Section 4.2 evaluates FIRE intrinsic variability. Section 4.3 evaluates the efficiency of steerable filter as compared with others. In Section 4.4, the pipeline is used to reproduce the previous literature results to test the image processing pipeline. Finally, Section 4.5 shows all the results for the analysis of real images using the pipeline chosen.

4.1 FIRE PIPELINE EVALUATION

The artificial collagen hydrogel images were created using the simulator program explained in Section 3.2. The aim of this analysis is to evaluate whether FIRE pipeline is able to compute faithfully the image network parameters.

All analysis was performed using a CPU with an Intel-Core i7- 4770 3.4 GHz processor and a 16 GB RAM.

Simulator routine runtime depends on the concentration of the collagen network of the image created. 1mg/ml collagen hydrogel images creation lasts for 5 minutes, while 2.5 mg/ml images creation may last for 20 minutes.

Twelve artificial images were created at the four collagen gel concentrations chosen (1-1.5-2-2.5 mg/ml) with the following inputs:

- Image volumes of size: 315x315x315 pixels.
- Pixel size of 0.225 μm in the three axes.
- Fibre diameter of 0.075 μm .
- Exponential fibre length distribution of the shape shown in Figure 19. Exponential distribution is set to reach a mean of 10.4 μm in artificial fibres' length.

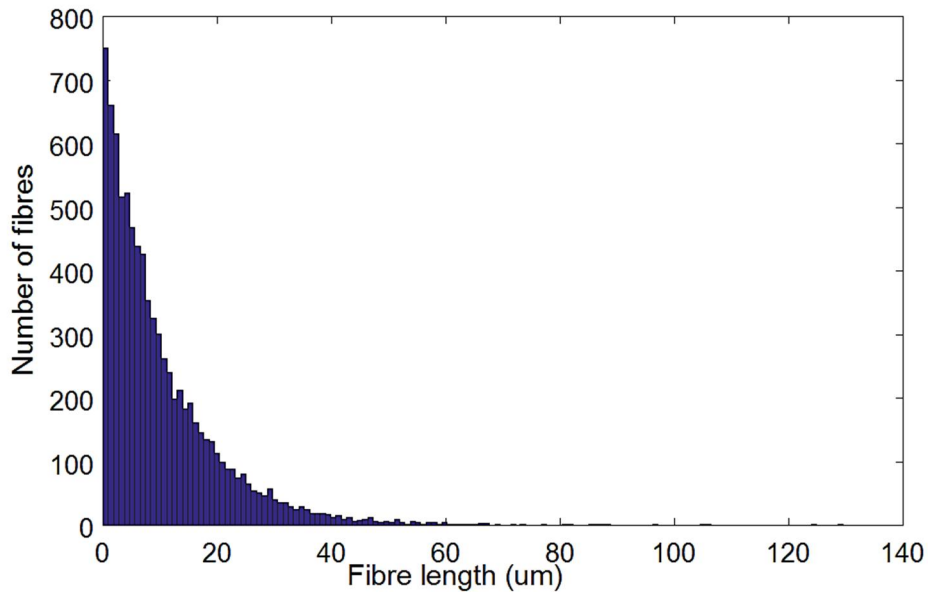


Figure 19: Exponential length distribution for artificial images.

In Figure 20, one example of synthetic images for each concentration are shown. However, these artificially generated images are the binary output of the simulator program, so it is necessary to get more realistic fibres, increasing their diameter, in order to implement the project's pipeline (binarization + FIRE).

Making the fibre network artificial image more realistic is a task that the simulator performs, as mentioned in Section 3.2, by applying a Gaussian smoothing to the network (see Figure 8). However, it was found out that the Gaussian smoothing produces a significant alteration on the length of the fibres. For that reason, we prefer another method to make the fibres look more natural that was to apply a dilation of the binary artificial image.

As shown in Figure 21, dilation gives fibres a broader body, with a smaller alteration of fibre length.

Once the artificial images were synthesized, they were processed using FIRE. The output results of FIRE for the network extraction of each artificial image are eventually compared to the input parameters for building the artificial network images.

In Figure 22 there is a visual resemblance comparison between an original simulated artificial volume and the its corresponding fibre network extracted for that artificial volume by FIRE.

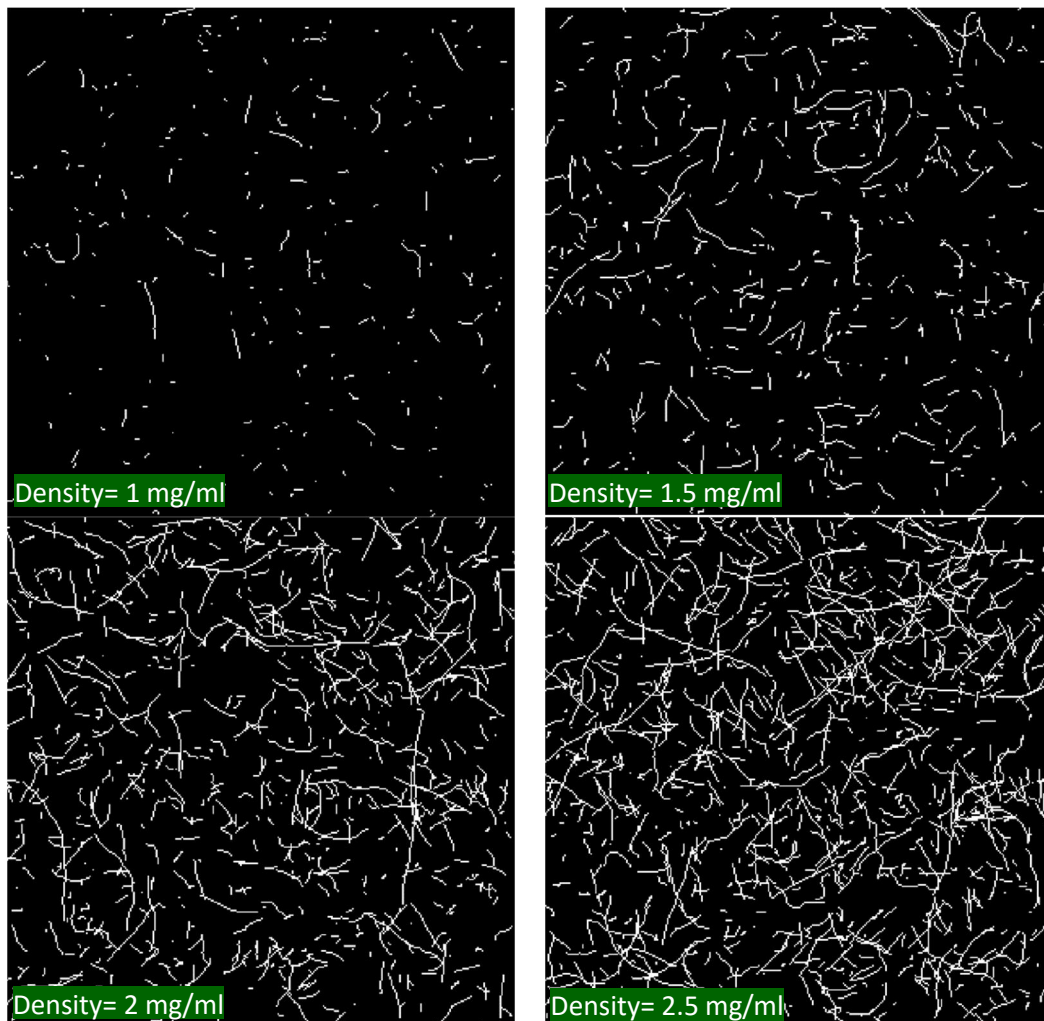


Figure 20: Artificial image examples at the four concentrations.

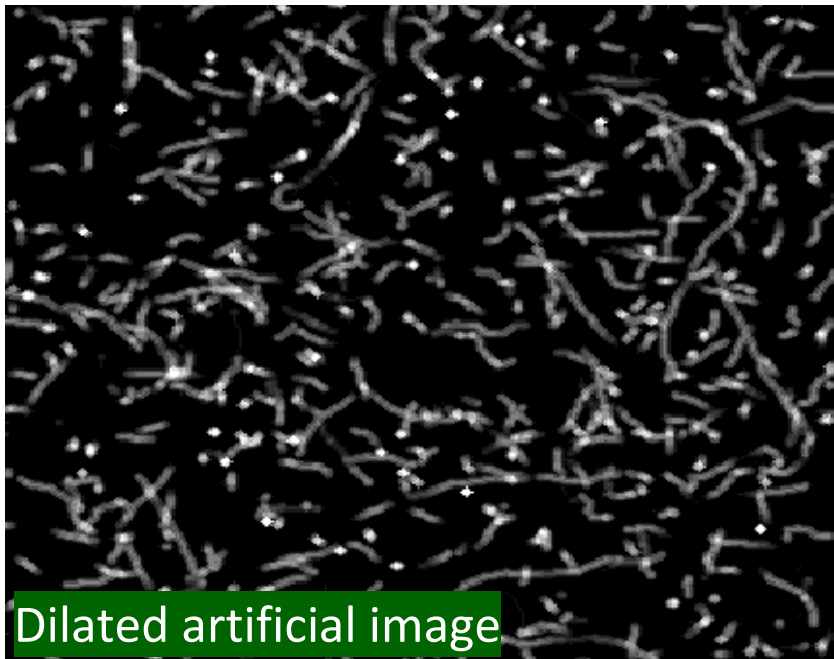
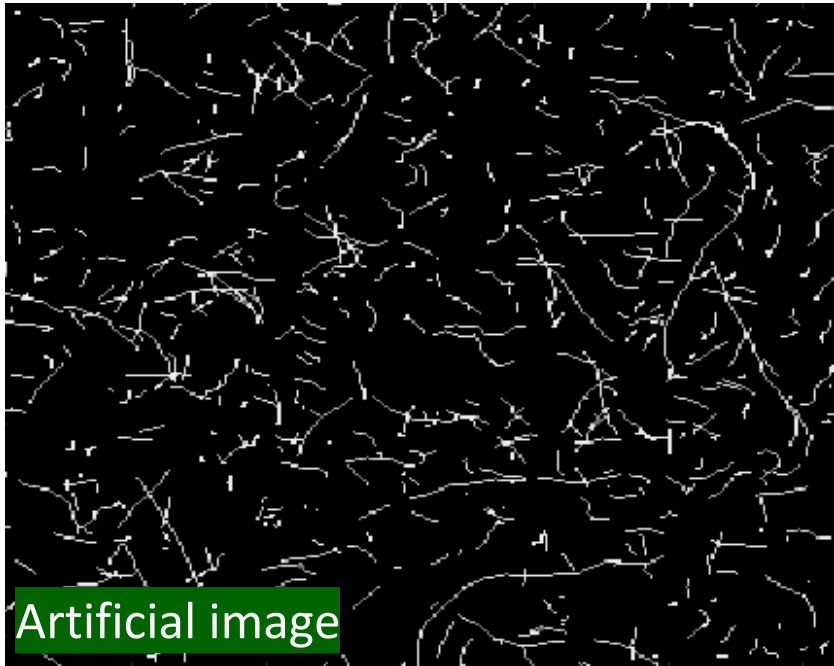


Figure 21: Artificial image dilation.

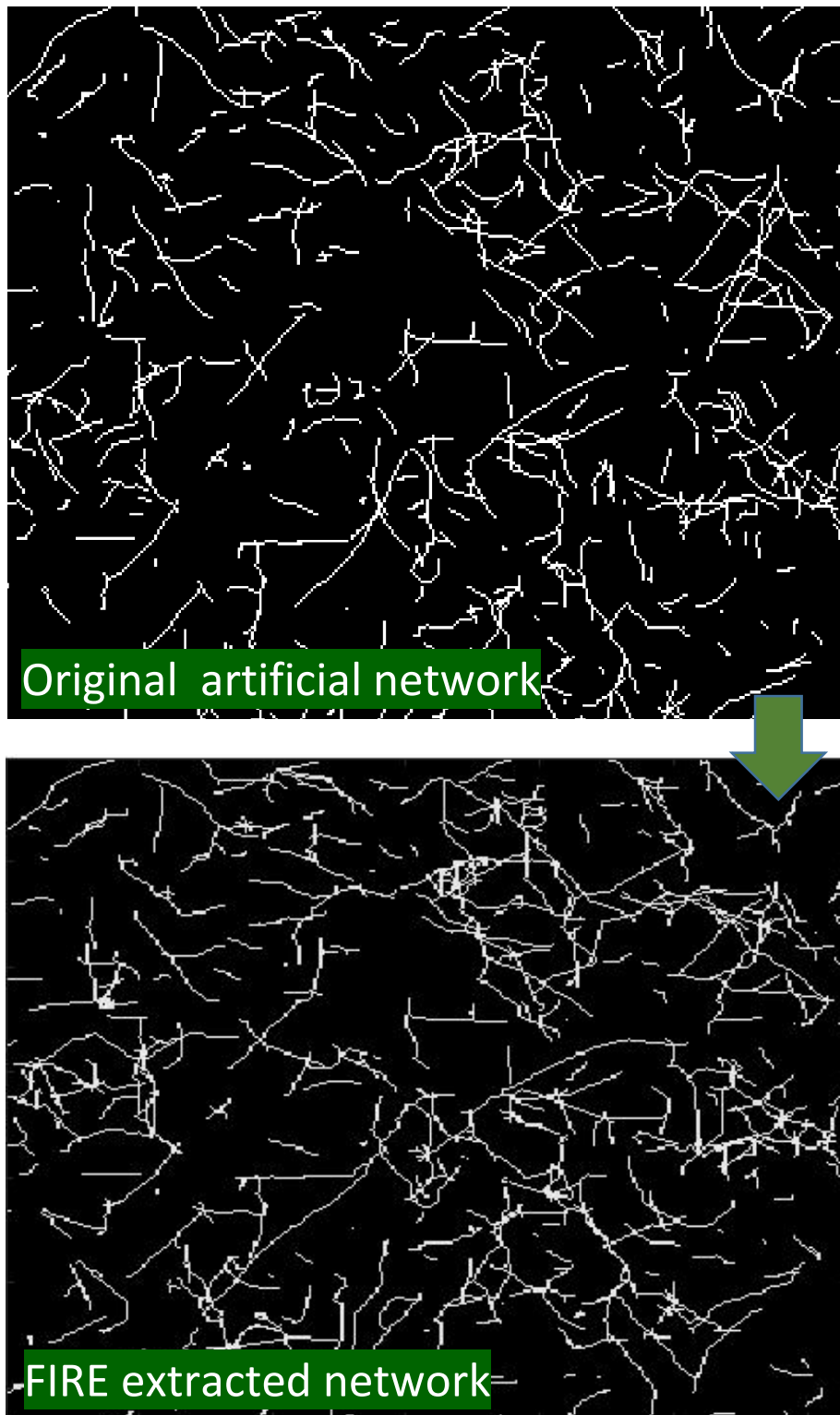


Figure 22: FIRE processing output

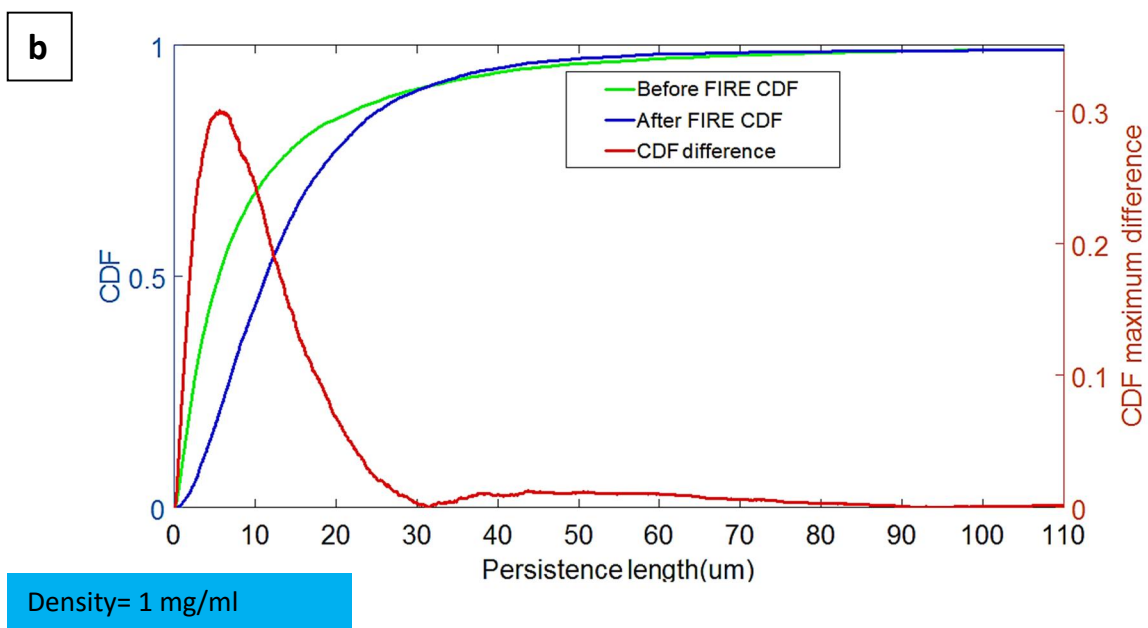
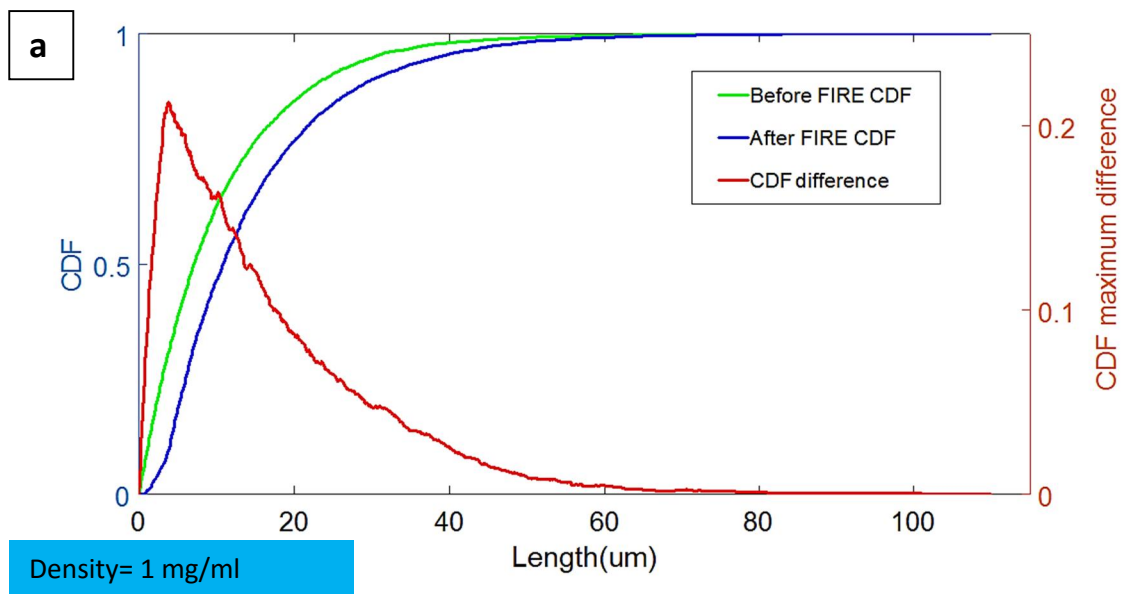
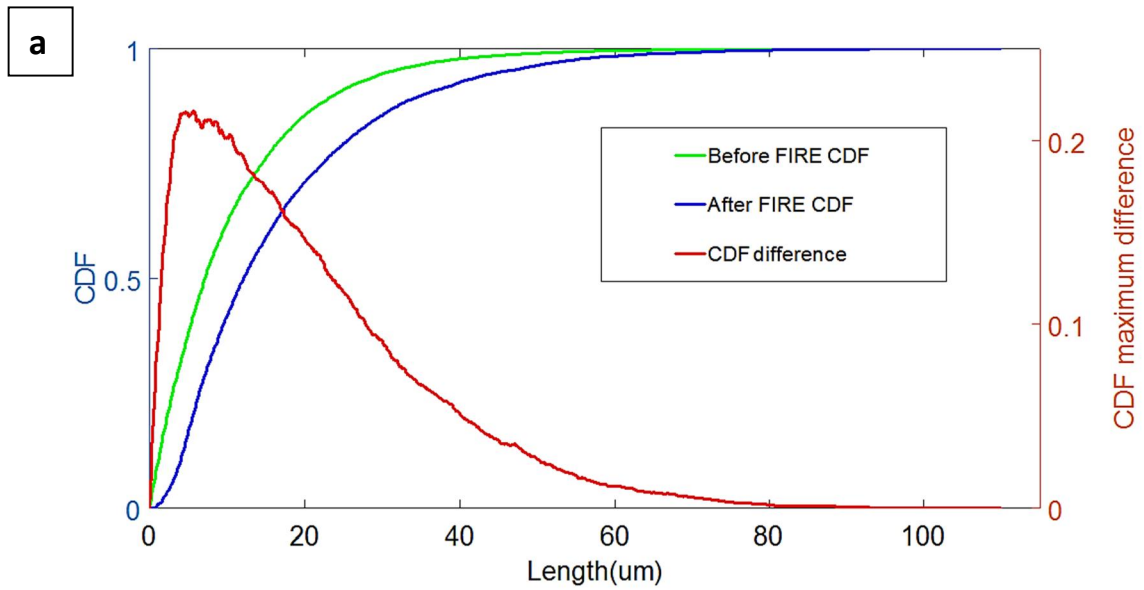
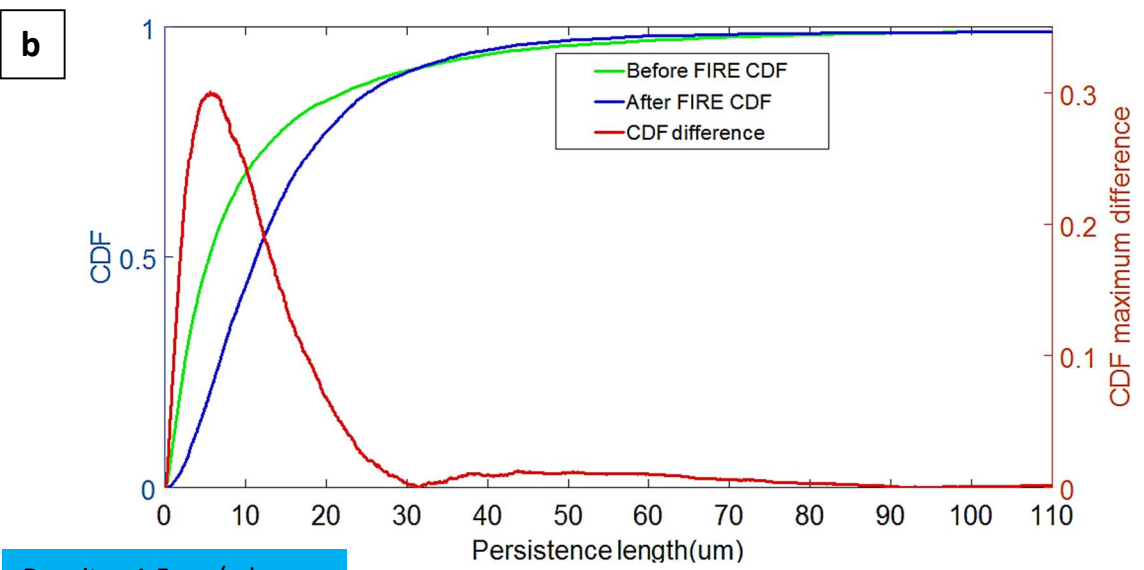


Figure 23: CDF distribution difference for fibre length and fibre persistence length between the original artificial image, and the results after FIRE processing: a) CDF difference in fibre length for density 1 mg/ml. b) CDF difference in fibre persistence length for density 1 mg/ml.

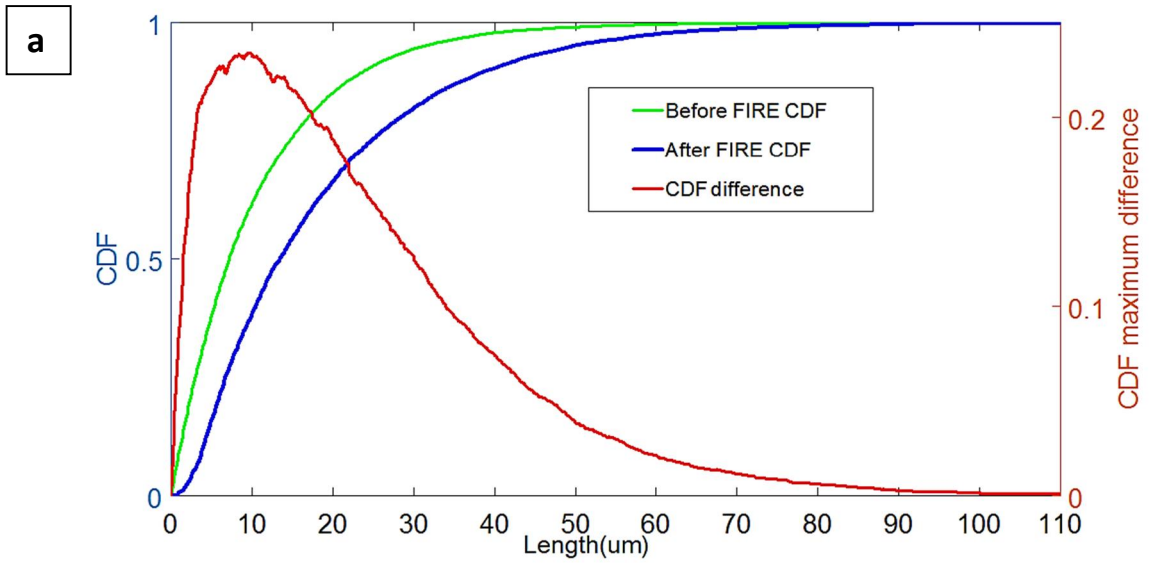


Density= 1.5 mg/ml

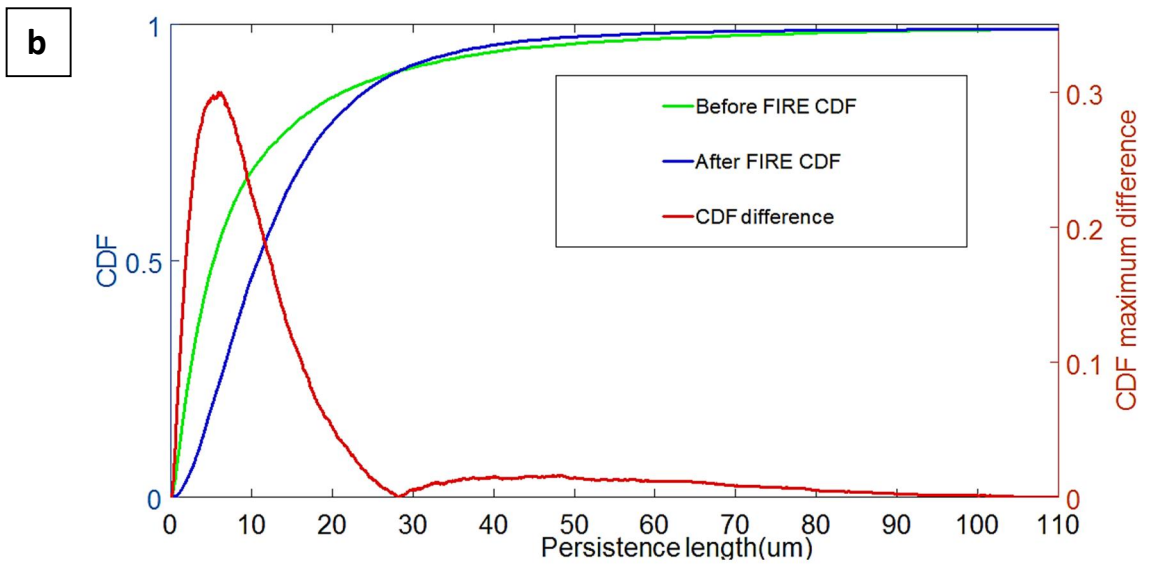


Density= 1.5 mg/ml

Figure 24 : CDF distribution difference for fibre length and fibre persistence length between the original artificial image, and the results after FIRE processing: a) CDF difference in fibre length for density 1.5 mg/ml. b) CDF difference in fibre persistence length for density 1.5 mg/ml.

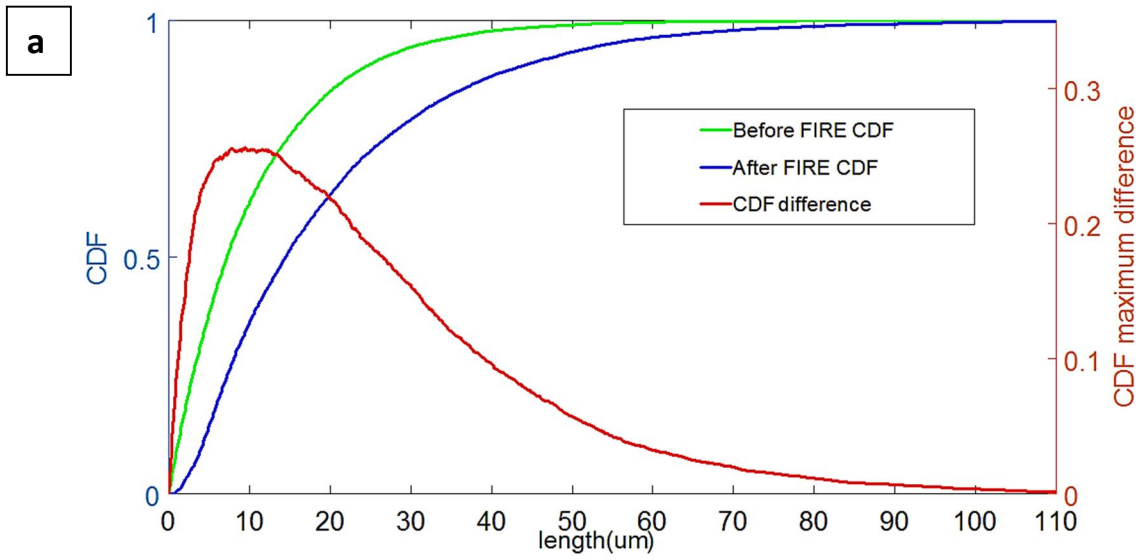


Density= 2 mg/ml

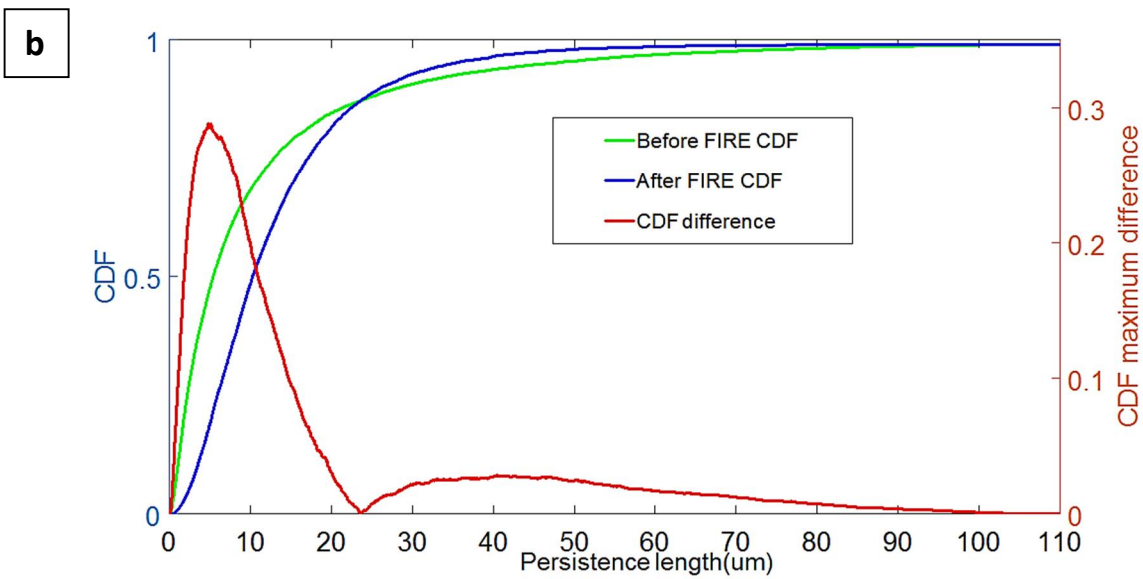


Density= 2 mg/ml

Figure 25: CDF distribution difference for fibre length and fibre persistence length between the original artificial image, and the results after FIRE processing: a) CDF difference in fibre length for density 2 mg/ml. b) CDF difference in fibre persistence length for density 2 mg/ml.



Density= 2.5 mg/ml



Density= 2.5 mg/ml

Figure 26 : CDF distribution difference for fibre length and fibre persistence length between the original artificial image, and the results after FIRE processing: a) CDF difference in fibre length for density 2.5 mg/ml. b) CDF difference in fibre persistence length for density 2.5 mg/ml.

Figures 23 to 26 show the difference between the cumulative distribution function (CDF) of fibre length and fibre persistence length's distribution (for each artificial image collagen density) between the original artificial image coming from the simulator (before FIRE) and the results obtained by the FIRE processing and parameters computation (after FIRE).

A mismatch between the original parameters and the parameter results after FIRE processing can be seen for all the concentrations. However, this is explained because artificial images have a very high number of small fibres due to their exponential length distribution (see Figure 19). The short fibres are removed by FIRE post-processing steps, triggering the mismatch between fibre length and fibre persistence length distributions.

Pore size computation was also performed for both the original artificial images and for the fibre network extracted for those images after FIRE processing. From the results of pore size shown in Table 4, it can be concluded that the difference between

Pore Size of artificial images (μm)			
Density (mg/ml)	Before FIRE	After FIRE	Difference
1	2.48	2.43	2%
1.5	2.05	1.94	5%
2	1.78	1.68	5.6%
2.5	1.6	1.5	6.25%

Table 4: Pore size difference between the original artificial images and the FIRE extracted networks.

the results of pore size after FIRE with respect to pore size before FIRE is quite low, less than 10 % for any of the concentrations.

This testing analysis shows that FIRE is a useful and reliable tool for the extraction and characterization of collagen fibre networks.

4.2 FIRE INTERNAL VARIABILITY

FIRE program bears some variability when computing the nucleation points of the same image on different runs of the software.

That variability is produced by the internal FIRE code that localizes the nucleation points in the image volume. There is an addition of random numbers to the distance function image, which results in a slight variation in the number of nucleation points found.

Consequently, in order to quantify how that nucleation points 'variation may affect our further analysis, a test was performed. That test consists on repeating three implementations of the same image, for 36 images. The maximum value of difference for the network computed parameters between similar implementations is shown in Table 5.

Parameter	Maximum Difference (%)
Nucleation point number	0.95
Fibre number	1.94
Fibre length mean	1.87
Fibre length median	2.49
Persistence length median	4.63
Pore size	6.89

Table 5: Maximum difference in parameters computation for similar implementations.

The values shown in Table 5 evidence that FIRE internal variability does not affect the final values for the parameters computation, hence it is not a problem to take into account.

4.3 PRE-PROCESSING FILTER TESTING

Binarization of collagen hydrogel's images is a critical step so as to end up with a proper extraction of the fibre network. Consequently, several filters were tested in real images in order to ensure that the steerable filter used is the most suitable one to remove the high amount of background noise of real collagen hydrogel images. An

inefficient noise removal may lead to wrong thresholding, which means incorrect binarization.

Three filters were tested for real images: Gaussian filtering of standard deviation equal to one, median filtering for five pixels' cubic sub-volumes and second order steerable filter of standard deviation equal to one. The parameters of the filters were chosen as to obtain the best performance.

As expected, it is shown in Figure 27 that the filter with better results is the steerable filter, both Gaussian and median filters do not lead to appropriate binarization. As it can be seen, Gaussian filter only blurs the fibres so it is tough to separate them in the thresholding; median filter is able to effectively remove background noise but the result is not useful for fibre extraction; while the second order steerable filter is able to enhance fibres and remove background noise so that thresholding step is effective in fibre extraction.

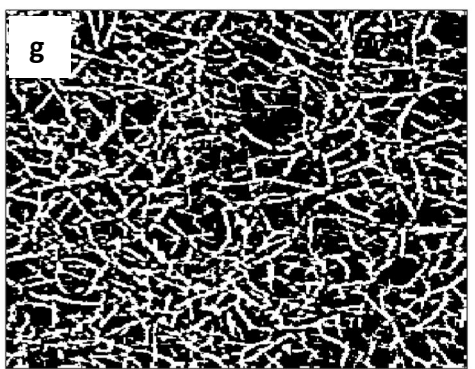
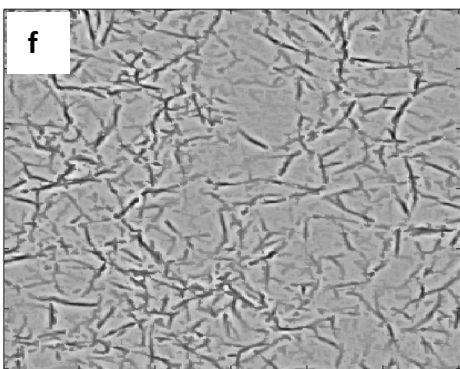
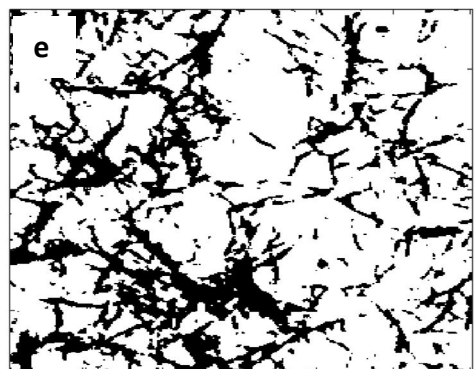
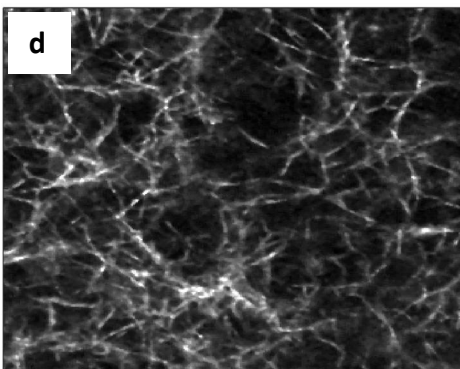
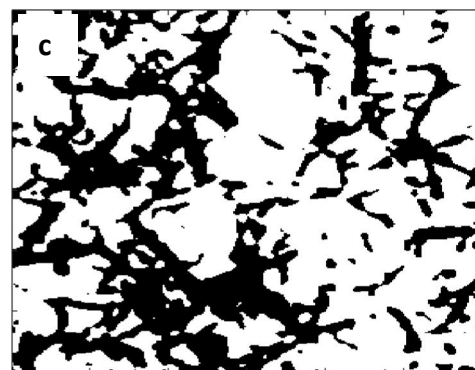
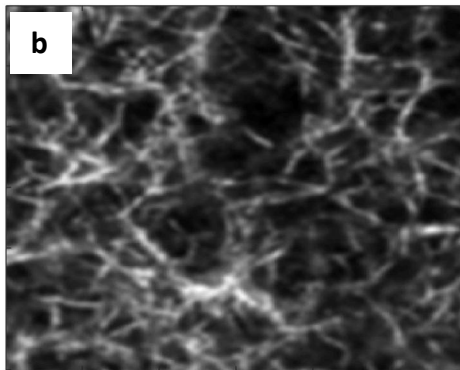
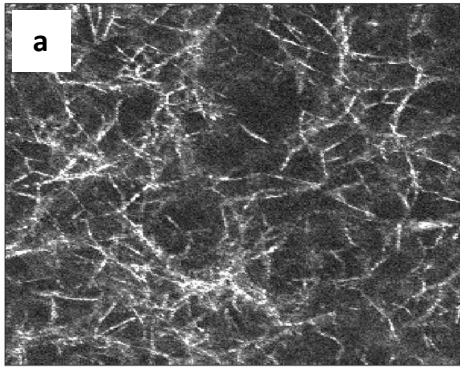


Figure 27: a) Real image. b) Gaussian filtered image. c) Otsu binarization of Gaussian filtered image. d) Median filtered image. e) Otsu binarization of Median filtered image. f) Steerable filtered image. g) Otsu binarization of steerable filtered image.

4.4 PIPELINE TESTING

Previous literature's images (mentioned in Section 3.3) were used in order to test the image analysis pipeline. That pipeline was extracted from Martin *et al.* paper [3], so we reproduced the same image analysis that was performed in that paper.

In Martin *et al.*'s work the three image datasets were binarized using the protocol explained in Section 3.5 (steerable filtering + Otsu thresholding) and then analysed using FIRE.

The comparison between the original results and the reproduction performed is shown in the Tables 6 to 8 and Figures 28 and 29.

	Fibre length (μm)		
Dataset	Martin <i>et al.</i>	Our results	Difference
I	4.32	4.60	6.5%
II	4.39	4.68	6.6%
III	4.51	4.67	3.5%

Table 6: Mean fibre length for the three image datasets.

	Fibre persistence length (μm)		
Dataset	Martin <i>et al.</i>	Our results	Difference
I	5.34	5.17	3.2%
II	5.57	5.07	9%
III	5.70	5.23	8.2%

Table 7: Median persistence length for the three datasets.

Dataset	Pore size (μm)		Difference
	Martin <i>et al.</i>	Our results	
I	4.14	4.07	1.7%
II	3.66	4.03	9.9%
III	4.25	4.67	9.9%

Table 8: Pore size mean for the three datasets.

Tables 6,7 and 8 include the original and the reproduced results for fibre length median, fibre persistence length median and network pore size median for the three collagen hydrogels image datasets. It can be noticed that the difference between the original results and the repetition implemented are quite low, results do not differ more than 10% in any of the cases. Moreover, these variations are totally random, they do not show any kind of pattern, and hence the pipeline for network extraction and characterization resulted to be robust and consistent.

Moreover, in Martin *et al.*'s paper, some figures help the visualization of the results. These graphs were reproduced and the outcome is shown in the Figure 28 and 29. The figures show the CDF distribution of the three datasets for fibre length and fibre persistence length respectively, plus the maximum difference between the CDFs in both cases. Repeated graphs follow the same pattern as the original ones; the three datasets keep similar CDF distribution for both parameters, so the maximum CDF difference does not reach 3% in any of the cases.

By the repetition of the results of Martin *et al.*'s paper, it can be concluded that the pipeline chosen is useful and reliable for the extraction and characterization of collagen fibre networks coming from collagen hydrogel's confocal reflection microscopy images.

From the reproduced analysis of this paper, it can be also mentioned that the three parameters studied (fibre length, fibre persistence length and pore size) are not affected by collagen gel composition in the three dataset analysed in this case as they remain almost constant.

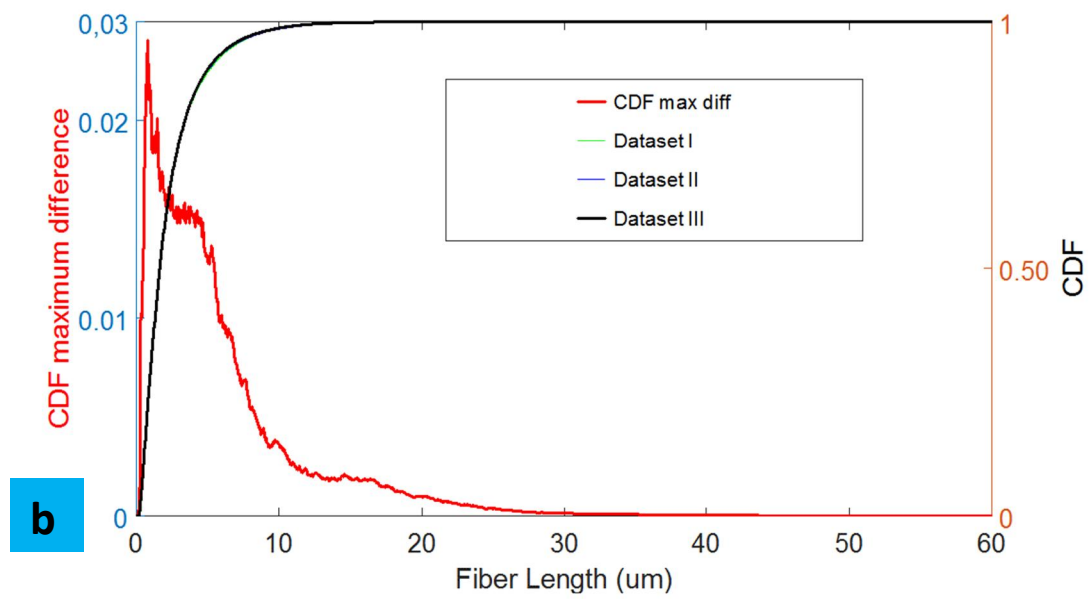
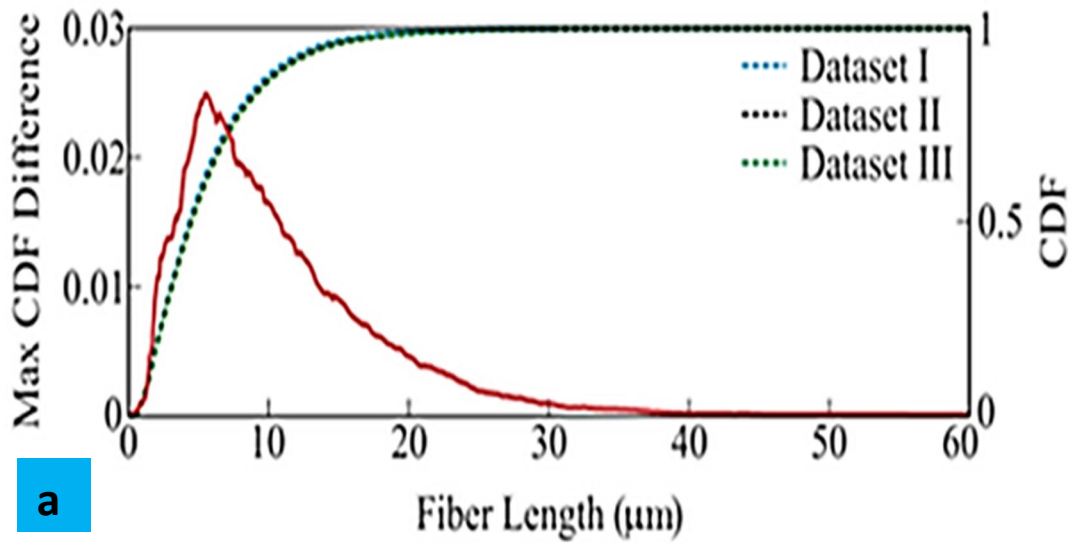
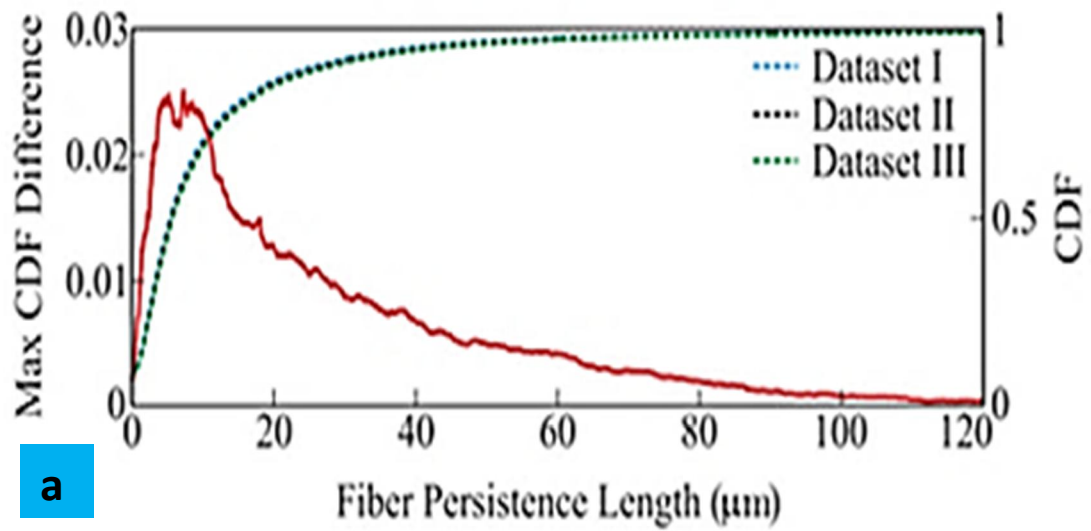
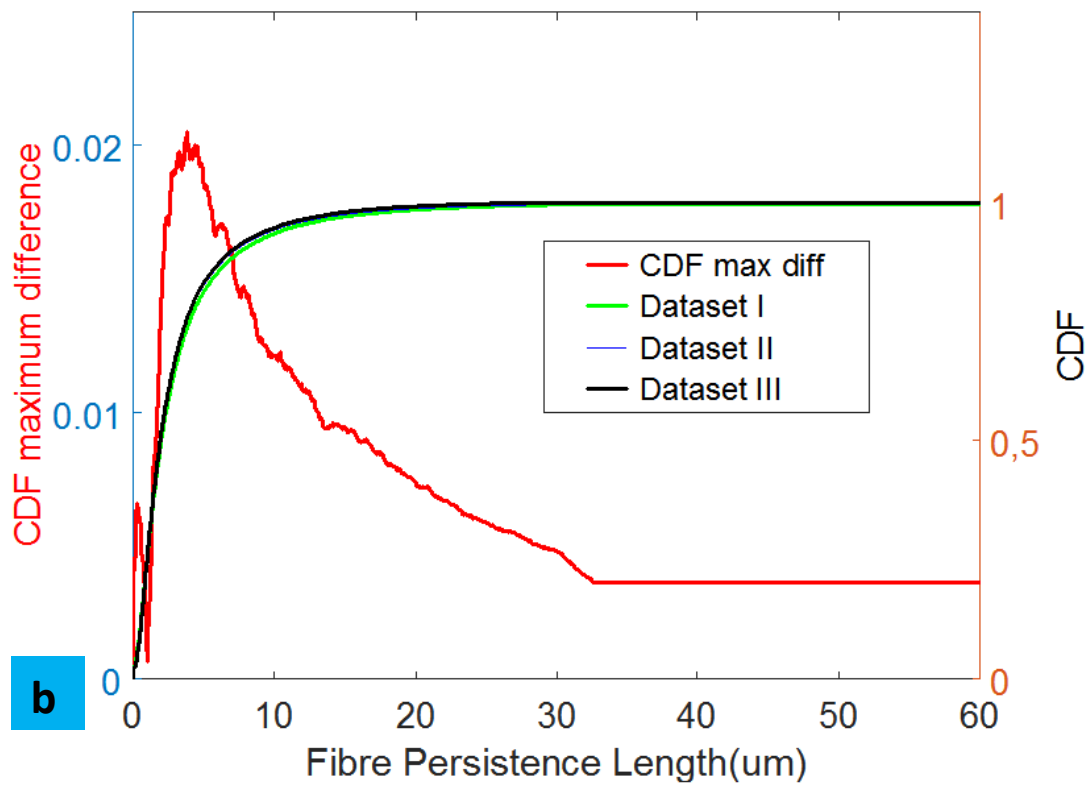


Figure 28 : Maximum CDF difference between the three datasets for fibre length. Original results (a) and reproduced results (b).



a



b

Figure 29: Maximum CDF difference between the three datasets for fibre persistence length. Original results (a) and reproduced results (b).

4.5 REAL IMAGES ANALYSIS

Once FIRE has been tested to be reliable and the processing pipeline has been shown to be consistent, the final step is to eventually use the proposed pipeline for the analysis of the real image volumes taken from the synthesized hydrogels.

As explained in Section 3.4, **12 image volumes for each of the hydrogel concentrations (1-1.5-2-2.5 mg/ml) were taken for gels polymerized inside culture wells and inside microfluidic devices and for the two microscopy techniques, confocal reflection and confocal fluorescence.**

Theoretically, reflection microscopy was used for normal collagen hydrogels and also confocal fluorescence microscopy was used for labelled collagen hydrogels. **However, the synthesis of fluorescently labelled collagen hydrogels was not fully developed,** and the quality of the labelling was not good enough. As it can be seen in Figure 30, the quality of confocal fluorescence images was not as good as desired. There is a high amount of background fluorescence noise due to free fluorophore that has not been correctly linked to collagen. Consequently, only confocal reflection microscopy images were used for the analysis.

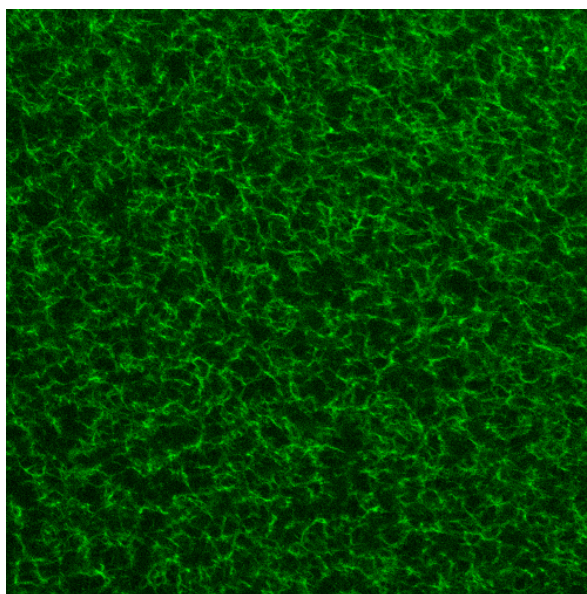


Figure 30 : Example of confocal fluorescence microscopy for collagen hydrogels.

To recapitulate in this project, **12 image volumes for each of the 4 collagen gel concentrations in culture wells and 12 image volumes for each of the 4 concentrations in microfluidic devices, taken with confocal reflection microscopy, are available for analysis with FIRE.** Examples are shown in Figure 31, where it can be seen that the collagen solutions have clearly polymerized to fibres both in culture wells and inside microfluidic devices.

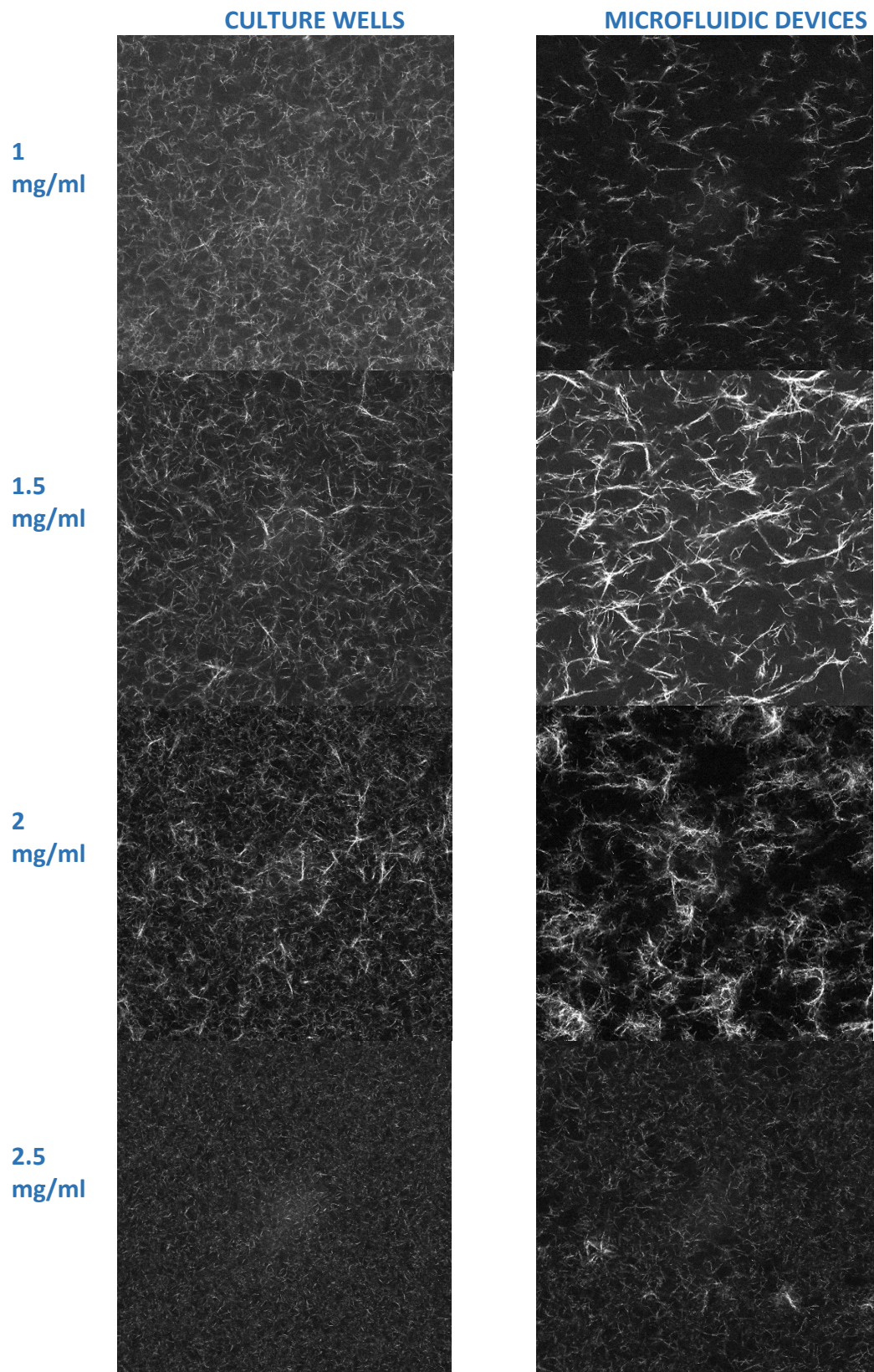


Figure 31: Examples of confocal reflection microscopy images for collagen hydrogels.

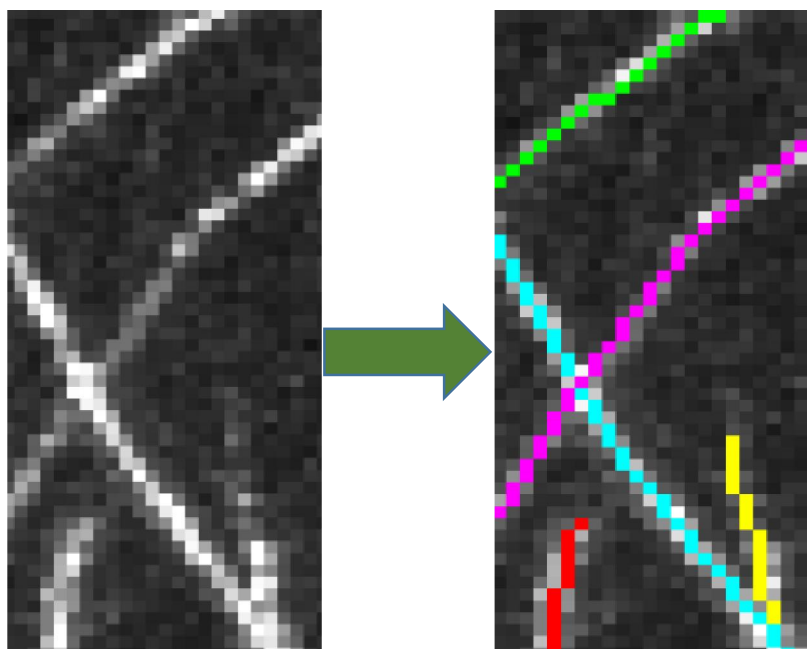


Figure 32 : Fibre extraction by FIRE [3].

In Figure 32 it can be seen an example of fibre extraction by the processing pipeline proposed for a real collagen hydrogel reflection microscopy image, each of the fibres identified is shown in a different colour.

Some results after the analysis of these images are showed by boxplots below. They were performed in order to show the differential distribution of fibre length mean, fibre persistence length mean, pore size mean and crosslink density for the 12 image volumes of each of the concentrations and for the two platforms (microfluidic devices and culture wells).

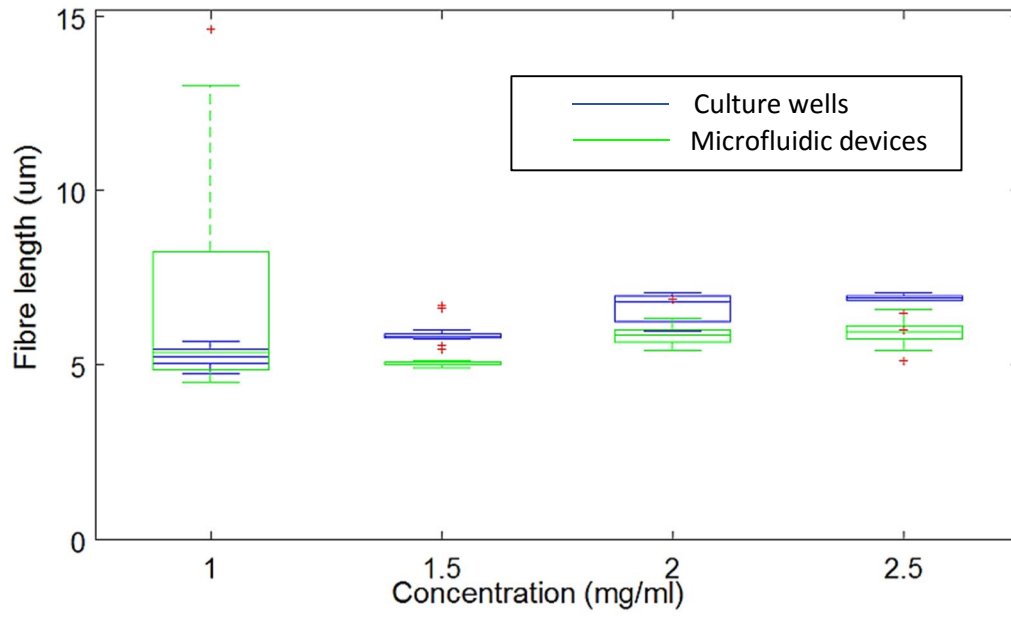


Figure 33 : Mean fibre length distribution vs concentration.

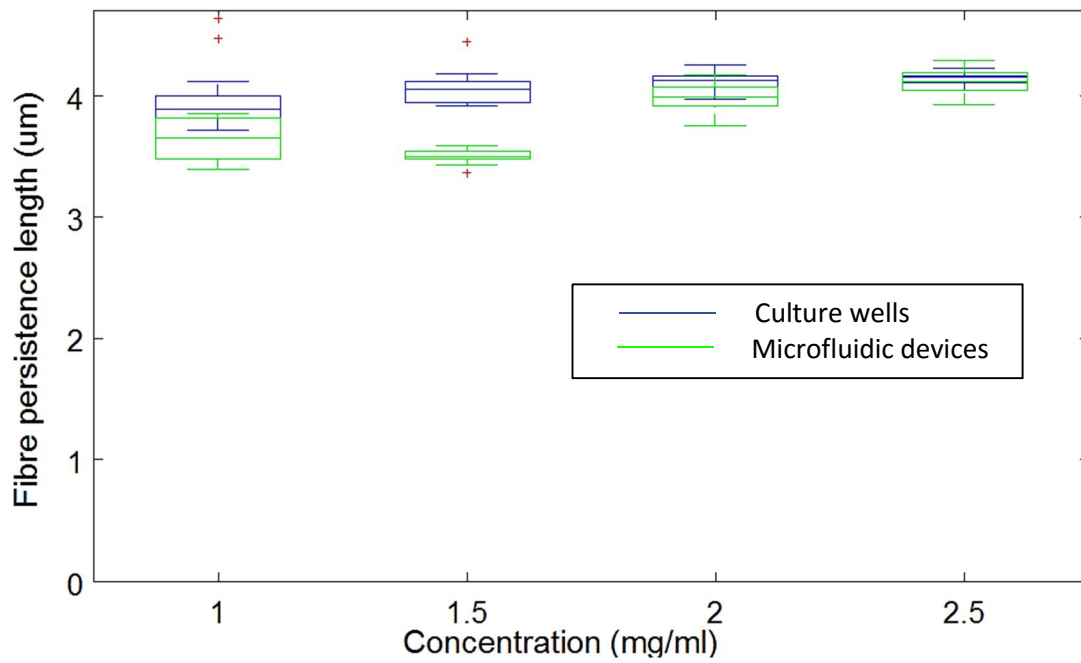


Figure 34 : Mean fibre persistence length distribution vs concentration.

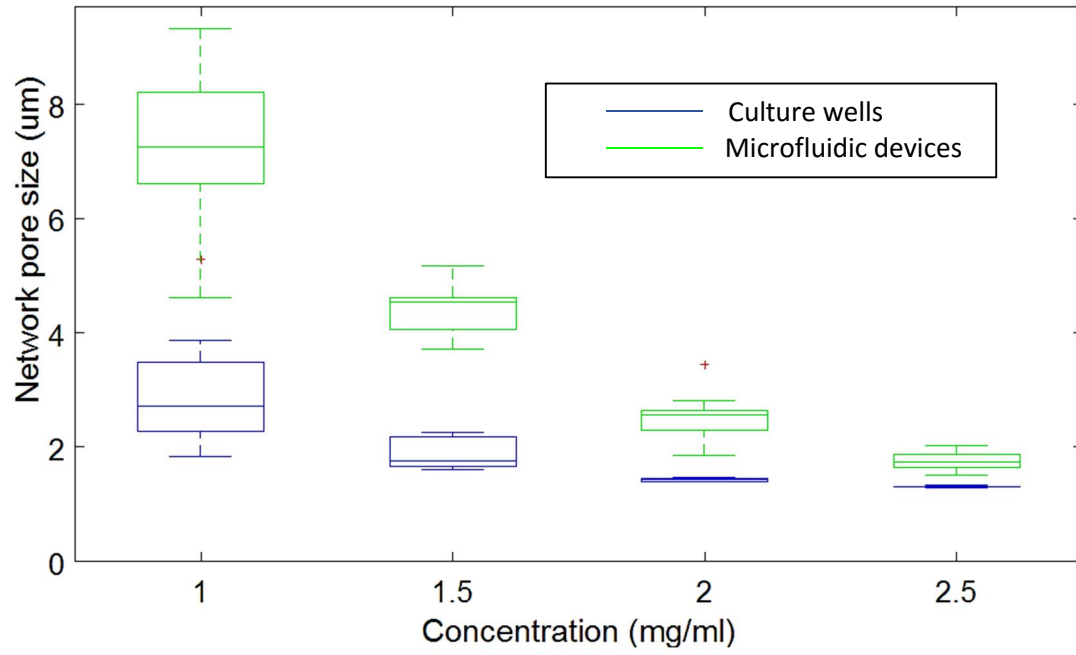


Figure 35: Mean pore size distribution vs concentration.

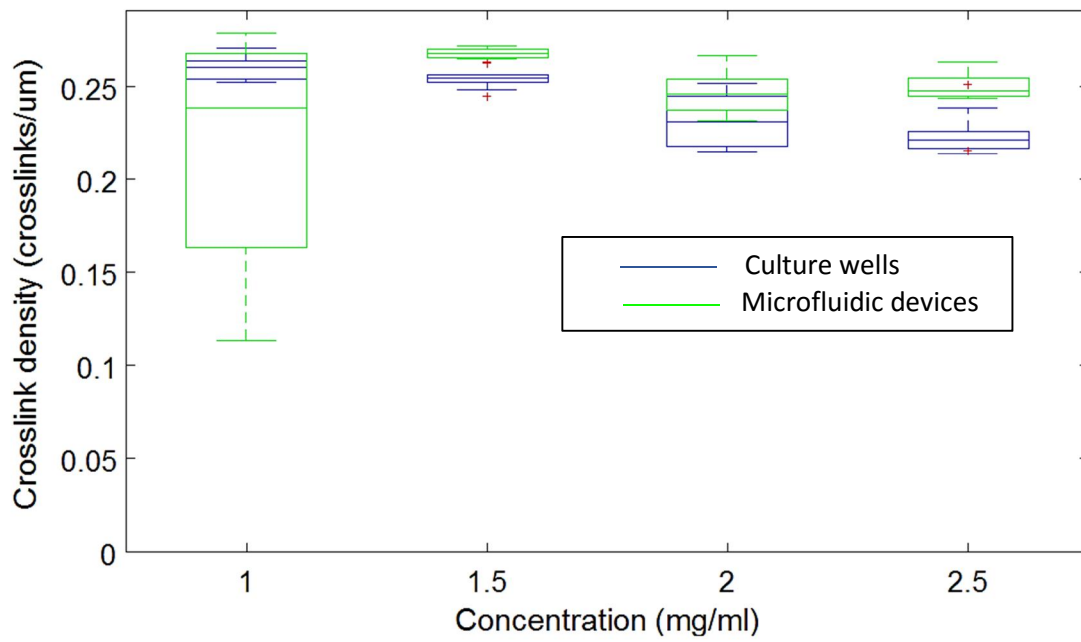


Figure 36: Crosslink density distribution vs concentration.

Fibre length distribution is shown in Figure 33. Images for the same concentration keep the same fibre length mean values, and even between all the concentrations the difference in fibre length mean is low. Moreover, there is not a big difference between the two platforms. Fibre length is kept almost constant for all the cases. The same behaviour is shown for persistence length mean (see Figure 34). So it can be concluded that fibre length and fibre persistence length do not seem to be affected by changes in the collagen concentration.

Meanwhile, pore size distribution (see Figure 35) shows a clear pattern of reduction, it does not keep constant. Pore size shrinks as concentration of the collagen hydrogel gets higher. That result is sensible as a higher gel concentration would leave less spaces in the network, thus pore size is smaller. It has to be pointed out as well the fact that pore size is higher in microfluidic devices than in culture wells. It may be explained because of the fact that when introducing the collagen solutions in the microfluidic devices through the inlets, some kind of directionality is induced to the collagen for polymerization. Hence fibres show a more directional pattern than in culture wells resulting in an increased pore size value.

Finally, crosslink density does not seem to change neither because of concentration nor for the platform used (see Figure 36). Despite of the fact that a higher concentration means more fibres in less space so crosslinks are more often forced to take place, total fibre length also increases. That produces a compensation leading to a more or less constant value for the crosslink density per unit length (see Section 3.1).

Processing pipeline runtime depends on the concentration of the collagen hydrogel of the image. FIRE last for a range of 1 hour to 4 hours, while pore size computation lasts for a range of 2 hours to 5 hours.

For the collagen concentration of 1 mg/ml inside the microfluidic devices, observe that the dispersion of the box plot for both the fibre length and the cross-link density is larger than for the other cases. We believe that it could be due to some issue with the polymerization of the collagen hydrogels so a repetition of the experiment is being performed.

5. CONCLUSIONS

- FIRE routine has been demonstrated to be a useful and reliable tool for the extraction of fibre network from collagen hydrogel microscopy images. There is a high fidelity between the original fibre networks and the ones retrieved by FIRE processing. Characterization of the network parameters is also possible thanks to FIRE and pore size computation algorithm, leading to substantial results.
- Proposed binarization and processing routine has turned up to be consistent for a proper extraction and characterization of fibre network from hydrogel's microscopy images. Real image's noise problem was solved by steerable filter.
- Real images analysis following the proposed processing pipeline show that both length and persistence length of the fibres seem to be not affected by the concentration of collagen of the hydrogel. In the other hand, pore size of the collagen network clearly suffers a reduction when concentration of the hydrogel increases.
- Both culture wells and microfluidics devices have been demonstrated to be useful as collagen hydrogel containing platforms. There is not a big difference in networks' parameters between the two platforms. Nevertheless, pore size of the network in microfluidic devices is larger than in culture wells, a difference that may be explained from the directionality of the fibres in microfluidic devices.

6. FUTURE WORK

- Collagen hydrogel's reflection images have an important drawback; fibre network is not complete because of the loss of the fibres that are perpendicular to the focal plane.

Confocal fluorescence microscopy sorts that problem out, as it enables the recognition of features perpendicular to the focal plane. However, this type of microscopy needs a fluorescent stain of the fibre network (see section 2.3.2). The main problem faced is the linkage of the fluorophore to the fibres. Using the protocol mentioned (Section 3.4.1.1), the efficiency of the fluorophore linkage was not strong enough, hence images have a high amount of background noise coming from free fluorophore (see Figure 30). Further work is needed to improve the protocol.

- The current software pipeline except for the pre-processing steerable filter is fully implemented in MATLAB resulting is a long computational time (i.e., several hours). It would be convenient to implement FIRE and the pore size estimation efficiently, for example, taking advantage of a multi-thread implementation.
- The study of collagen hydrogels inside **culture wells and microfluidics devices** is not trivial. Both platforms are widely used for cellular studies, which is the final objective of this research line. Observing the interactions between ECM, (represented as collagen hydrogels) and cancer cells embedded inside and their consequences in cancer cell fate could arise in interesting results that may help cancer understanding or may be useful for developing new cancer drugs. Microfluidic devices use is specially stirring as they allow to control the input substances that cancer cells receive as well as waste removal, or even the forces and flows exerted to the cells. That feature is especially advantageous when observing differential cancer cell behaviour depending on the environmental conditions.

7. SOCIOECONOMIC IMPACT

As mentioned in the motivation of this bachelor thesis (Section 1.1), cancer is one of the principal causes of death in the world, especially in first world countries. Current most prevalent cancer treatments are based on killing cancer cells by X-ray irradiation or chemical destruction. However, this type of treatments is non-selective so they usually affect normal cells as well, leading to terrible side-effects in cancer patients. Consequently, cancer pharmacological industry companies are now gathering their efforts in developing drugs that reduce side-effects by only acting in tumoral cells. For that purpose, it is important to identify specific features of cancer cells that can be attacked to hinder tumour progression. The most important path of research is to study the genes that inhibit cancer progression so as to enhance them or those genes which activate cancer progression in order to repress them. Nevertheless, it is important to take into account that cancer progression holds a huge complexity, and it is mainly governed by the interactions between extracellular matrix components and cancer cells (Section 1.2.2).

FIRE fibre extraction algorithm is useful for the extraction of network disposition and characterization of fibre network parameters from microscopy image volumes taken of ECM models. That allows the analysis of ECM networks with cancer cells embedded, and hence, study how cancer cell progression is affected by ECM and vice versa. The final objective is to develop drugs that specifically act on cancer cells or their environment to stop tumour progression.

This project has a great potential in terms of value for society, as it is aimed to help on cancer research and drug development. Consequently, this support could end up with one of the main scourges in today's society health.

8. BUDGET

<i>Experimental cost (hydrogels)</i>			
<i>Description</i>	<i>Number of units</i>	<i>Cost per unit (€)</i>	<i>Total cost (€)</i>
Collagen I rat tail	1	219.37	219.37
Micropipettes kit	1	637.67	637.67
Culture wells	1	141.49	141.49
Microfluidic devices	12	30.00	360.00
Total cost			1,358.53 €
<i>Experimental costs (microscopy)</i>			
<i>Description</i>	<i>Number of hours</i>	<i>Cost per hour (€)</i>	<i>Total cost (€)</i>
Microscopy sessions	27	7.00	189.00
Total cost			189.00 €
<i>Processing cost</i>			
<i>Description</i>	<i>Number of units</i>	<i>Cost per unit (€)</i>	<i>Total cost (€)</i>
Computer	1	1,000.00	1,000.00
MATLAB license	1	2,000.00	2,000.00
Total cost			3,000.00 €
<i>Labour costs</i>			
<i>Description</i>	<i>Number of hours</i>	<i>Cost per hour (€)</i>	<i>Total cost (€)</i>
Student	400	5.50	2,200.00
Supervisor	75	15	1,125.00
Tutor	50	30	1,500.00
Laboratory chemist	75	15	1,125.00
Microscopy technician	27	30	810.00
Total cost			6,760.00 €
TOTAL PROJECT COST			11,307.53 €

Table 9 : Bachelor thesis budget.

9. ANNEX I (INPUT FIRE PARAMETERS)

Parameter	Function	Values
σ_d	Standard deviation of smooth distance function	0.3
Dtype	Type of distance function	'cityblock'
Θ_{nuc}	Distance function threshold for a point to be NP	1.5
S_{xbox}	Radius of the box to find NP	5
Θ_{LMP}	Distance function threshold for a point to be LMP	0.2
$\Theta_{LMPdist}$	Maximum distance to fuse two LMPs	2
Θ_{EXT}	Maximal value of the angle between the direction of the fibre and the direction of the candidate extension	$\cos\left(\frac{7\pi}{180}\right)$ rad
$\lambda_{dirdecay}$	Decay rate for fibre direction update	0.5
Θ_{dang-L}	Fibre is removed if it is shorter than his value (in pixels)	15
$\Theta_{dang-extend}$	Maximum difference in angle between a short fibre such that it is considered to be aligned with another fibre going through the same cross-link	$\cos\left(\frac{10\pi}{180}\right)$ rad
$S_{fibredir}$	Number of nodes used for calculating direction of fibre end	4
Θ_{linkd}	Maximal distance between two fibres ends for which the fibres may be linked	8
Θ_{linka}	Minimum angle between two fibre ends for linking of the two fibres	$\cos\left(\frac{-130\pi}{180}\right)$ rad
Θ_{numv}	Minimal fibre length for a fibre with one or zero crosslinks. shorter fibres are removed	3
Θ_{flen}	minimum length of a free fibre	15

10. BIBLIOGRAPHY

- [1] Mathers C., Boschi-Pinto C., Lopez A. and Murray C. World Health Organization: Cancer incidence, mortality and survival by site for 14 regions of the world. 2012. Retrieved in: http://www.who.int/gho/ncd/mortality_morbidity/cancer/en/.
- [2] Stein AM, Vader D., Jawerth L., Weitz D. and Sabder L. (2008). An algorithm for extracting the network geometry of three-dimensional collagen gels. *J. Microscopy*, 232 (3) 463-475.
- [3] Maska M., Ederra C., Fernández-Marqués J., Muñoz-Barrutia A., Kozubek M. and Ortiz de Solórzano C. (2015). An algorithm for extracting the network geometry of three-dimensional collagen gels. *Proc. of the International Conference on Image processing (ICIP'15)*, 1791-1794.
- [4] Gelse K., Weaver V. and Aigner T. (2003). Collagens—structure, function, and biosynthesis. *Advanced Drug Delivery Reviews*, 55 ,1531– 1546.
- [5] Alberts B., Bray D., Hopkin K., Johnson A., Lewis J., Raff M., Roberts K. and Water P. (2004). *Essential Cell Biology* (2nd edition). Spain: Garland Science.
- [6] Chon S. (2014). Extracellular components and connections between cells. [Figure]. Retrieved in: <https://prezi.com/l1plaxtrq51d/extracellular-components-and-connections-between-cells/>.
- [7] Lu P., Boschi-Pinto C., Lopez A. and Werb Z. *JCB: The extracellular matrix: A dynamic niche in cancer progression*. 2012. Retrieved in: <http://jcb.rupress.org/content/196/4/395.figures-only>.
- [8] Samarasinghe B. (2013). Invasion and Metastasis. [Figure]. Retrieved in: <http://blogs.scientificamerican.com/guest-blog/the-hallmarks-of-cancer-6-tissue-invasion-and-metastasis/>.
- [9] McBeath R., Pirone DM., Nelson CM., Bhadriraju K, and Chen CS. (2004). Cell shape, cytoskeletal tension, and RhoA regulate stem cell lineage commitment. *Dev Cell*, 6(4):483-95.
- [10] Wu J., Rajwa B., Filmer D., Hoffmann CM, Yuan B., Chiang CS., Sturgis J. and Robinson JP. (2003). Analysis of Orientations of Collagen Fibres by Novel Fibre-Tracking Software. *Microsc. Microanal.* 9, 574–580.
- [11] Mickel W., Münster S., Jawerth LM., Vader D., Weitz D., Sheppard A., Mecke K., Fabry B. and Schröder-Turk G. (2008). Robust Pore Size Analysis of Filamentous Networks from Three-Dimensional Confocal Microscopy. *Biophys J.* 95(12): 6072–6080.
- [12] Lang N., Münster S., Metzner C., Krauss P., Schürmann S., Lange J., Aifantis K., Friedrich O. and Fabry B. (2013). Estimating the 3D Pore Size Distribution of Biopolymer Networks from Directionally Biased Data. *Biophys J.* 105(9): 1967–1975.

- [13] Bradshaw A. (2009). Pressure Overload–Induced Alterations in Fibrillar Collagen Content and Myocardial Diastolic Function. [Figure]. Retrieved in: <http://blogs.scientificamerican.com/guest-blog/the-hallmarks-of-cancer-6-tissue-invasion-and-metastasis/>.
- [14] Department of Biology Memorial University of Newfoundland (2015). Principles of Cell Biology (BIOL2060). [Figure]. Retrieved in: <http://www.mun.ca/biology/desmid/brian/BIOL2060/BIOL2060-17/CB17.html>.
- [15] Paleos, G. Pittsburgh Plastics Manufacturing: What are hydrogels? 2012. Retrieved in: sburghplastics.com/assets/files/What%20Are%20Hydrogels.pdf.
- [16] Cornell University Centre on the microenvironment and metastasis: Microfluidic devices, 2013. Retrieved in: http://cmm.cornell.edu/files/all/microfluidics_sample_for_website_1.pdf.
- [17] Barr V. and Bunnell S. (2010). Interference Reflectance Microscopy. Curr Protoc Cell Biol. CHAPTER: Unit–4.23.
- [18] Semwogerere D. and Weeks E. Emory University: Confocal Microscopy, 2005. Retrieved in: www.physics.emory.edu/~weeks/lab/papers/ebbe05.pdf.
- [19] Johnston D. and Page A. (2006). Confocal Microscopy - principles and applications [Figure]. Retrieved in: <https://www.som.soton.ac.uk/research/sites/biu/group/GroupConfocalWeb.pdf>.
- [20] Purdue University Cytometry Laboratories. How Does Digital Imaging Relate to Microscopy? [Figure]. Retrieved in: http://www.cyto.purdue.edu/cdroms/micro1/7_spon/vaytek/faq.htm
- [21] Moscow State University Physics Department: Ideal polymer chains. Retrieved in: <http://polly.phys.msu.ru/ru/education/courses/polymer-intro/index.html/lecture2.pdf>.
- [22] Corning Inc. Corning Matrigel matrix: Cells behave better on Corning Matrigel matrix. Retrieved in : <https://www.corning.com/au/en/products/life-sciences/products/surfaces/matrigel-matrix.html>.
- [23] Shin Y., Han S., Jeon J., Yamamoto K., Zervantonakis I., Sudo R., Kamm R. and Chung S. (2012). Microfluidic assay for simultaneous culture of multiple cell types on surfaces or within hydrogels. Nat Protoc. 7(7): 1247–1259.
- [24] Freeman W. and Adelson E. (1991). The Design and Use of Steerable Filters. Trans. Patt. Anal. and Machine Intell. Vol. 13, No. 9, pp. 891-906.
- [25] Aguet F. 2D Steerable filters for feature detection. [Figure]. Retrieved in: <http://www.francoisaguet.net/software.html>.
- [26] Turkel E. Math department Tel Aviv University: Automatic thresholding. Retrieved in: <http://www.math.tau.ac.il/~turkel/notes/otsu.pdf>.